Spring 4-20-2018

Effect of Shot Peening on Stress Corrosion Behavior of Biodegradable Magnesium WE43

Tejaswita Patil
University of Nebraska - Lincoln, tejaswita.patil@huskers.unl.edu

EFFECT OF SHOT PEENING ON STRESS CORROSION BEHAVIOR OF BIODEGRADABLE MAGNESIUM WE43

by

Tejaswita Patil

A THESIS

Presented to the Faculty of

The Graduate College at the University of Nebraska

In Partial Fulfillment of Requirements

For the Degree of Master of Science

Major: Mechanical Engineering and Applied Mechanics

Under the Supervision of Professors Florin Bobaru and Michael Sealy

Lincoln, Nebraska

April, 2018

EFFECT OF SHOT PEENING ON STRESS CORROSION BEHAVIOR OF BIODEGRADABLE MAGNESIUM WE43

Tejaswita Patil, M.S.

University of Nebraska, 2018

Advisors: Florin Bobaru and Michael Sealy

Conventionally used metals for orthopedic devices made of titanium, stainless steel, and Co-Cr alloys are designed to be permanently implanted. However, long-term complications arise and a secondary implant removal surgery is often necessary. A mismatch in stiffness between the bone and implant results in stress shielding that negatively affects bone density. To overcome these problems, magnesium alloys (*e.g.*, WE34) are favored due to a lower Young's modulus (45 GPa) and biodegradability. The critical technical barrier with magnesium alloys is their high corrosion rate in physiological (salt-based) environments. One solution is to use surface treatments, such as shot peening (SP), to induce surface residual stresses and slow the degradation rate. The corrosion rate can be customized according to patient specific parameters, such as age and bone health, or application (*i.e.*, pelvic fracture *vs.* spinal fracture) through SP process parameter manipulation (*e.g.*, peening pressure). However, the effect of residual stresses from SP on stress corrosion behavior of magnesium alloys remains inconclusive. The purpose of this study is to evaluate the effect of shot peening with different peening pressures on the stress corrosion rate of WE43 using polarization tests. The results for this study indicate that the corrosion resistance of the alloy increased as the pressure of shot peening increased and is inversely proportional to the applied external load. A relation between the surface integrity and the stress-corrosion behavior of the shot peened samples has been found.

DEDICATION

I dedicate this work to my parents, Shripati and Namrata Patil, my brother Gaurav Patil, and my sister-in-law Teja Karkhanis. They have always encouraged me to carve out my own path and achieve my goals. I also dedicate this to Amal Ponathil, whose love, humor, and support has kept me optimistic in every difficult situation. Finally, I dedicate this work to Dr. Michael Sealy, whose kindness, patience, and positive attitude has made me a better person.

ACKNOWLEDGEMENTS

I would like to express my appreciation to both of my advisors, Dr. Florin Bobaru and Dr. Michael Sealy. This work would have been impossible without their encouragement and wisdom, and I could not be more appreciative.

I would also like to thank Shumin Li for helping me with corrosion testing; Wenlong Li and Zesheng Zhang for providing tensile test training; Jay Taylor for helping with identifying microstructure characterization; and Dr. Shah Vallopilly for X-Ray diffraction training. I would like to express my special thanks to the Physics department instrument shop team, who assisted me in manufacturing components for my experiments. Lastly, I would like to thank my fellow colleagues: Haitham Hadidi, Cody Kanger, Guru Charan Reddy Madireddy for offering their guidance and expertise at every stage of my research. I would also like to thank my roommate and colleague Sneha Akula for being my partner in this emotional journey.

This work has been supported by the ONR project N00014-15-1-2034, “SCC: The Importance of Damage Evolution in the Layer Affected by Corrosion” (Program Manager: William Nickerson).

LIST OF ABBREVIATIONS AND SYMBOLS

MPa	Megapascal
N	Newton
R_a	Surface roughness (arithmetic mean)
R_v	Valley roughness
R_p	Peak roughness
SCC	Stress corrosion cracking
PDP	Potentiodynamic polarization
k	Spring constant
F	Force applied by spring
x	Displacement of spring
d	Lattice spacing
cfm	Cubic feet per minute
σ_{max}	Maximum permissible axial stress
SP	Shot peening
LSP	Laser shock peening
VHN	Vickers hardness number
σ_{SCC}	Threshold stress
K_{ISCC}	Threshold stress intensity factor
V	Steady stress corrosion crack velocity
K_I	Stress intensity factor at crack tip
Y	Geometric factor

σ	Applied stress
a	Crack length
ρ	Density
u	Displacement
$\ddot{u}$	Acceleration
b	Body forces
t	Time
H_x	Horizon
δ	Radius of horizon

CONTENTS

LIST OF TABLES

LIST OF FIGURES

CHAPTER 1

MAGNESIUM AS A BIOMATERIAL

1.1 Magnesium Alloys as Orthopedic Biomaterials

1.1.1 History of Magnesium for Biomaterials

The history of metallic magnesium dates back to the 19th century, when Sir Humphry Davy first discovered it in elemental form. His assistant, Michael Faraday, implemented the electrolysis of fused anhydrous $MgCl_2$ in 1833 [1]. Nearly 45 years later (c. 1878), magnesium was first used as an implant material when Edward C. Huse used magnesium (Mg) wires as ligatures to successfully stop bleeding vessels in radial arteries and in operations of varicocele on three patients. It was observed that Mg wires were not ductile enough for biomedical purpose. In 1900, Dr. Erwin Payr experimented on different shapes of high-purity thin walled magnesium cylinders as connectors for vessel anastomosis [2]. Many scientists later investigated the use of different magnesium alloys with different geometries on humans and animals (such as rabbits, pigs); and thus, began the expedition of using magnesium alloys as biomaterials.

1.1.2 Problems with Current Permanent Metal Alloys

Metallic materials are commonly used in orthopedic implant surgeries to repair or replace diseased or damaged bone tissue. Due to the combination of excellent mechanical strength and fracture toughness, metals are preferred over polymers and ceramics for load bearing applications. Currently approved metals for various biomedical purposes include titanium (Ti), stainless steel (SS), and cobalt-chromium (Co-Cr) alloys. Some of these

metals release metallic ions which can have a long-term chronic effect. Moreover, these materials have a higher elastic modulus and stiffness as compared to human bone. As a consequence, stress shielding is observed in bones due to the imbalance of these properties that leads to reduced stimulation of osteogenesis or decrease in bone density with time, thus reducing implant stability [3, 4].

Traditionally used metals, such as Ti-, SS-, and Co-Cr alloys, are considered bio-inert materials *in vivo*. Although bio-inert does not truly exist, these materials remain permanent fixtures within the body and result in complications requiring another surgery. Unfortunately, a secondary implant removal surgery is often required due to permanent physical irritation or inflammatory discomfort from permanent implantation. This implant surgery increases the cost of healthcare and increases the risk of morbidity for patients [5].

1.1.3 A Biodegradable Alternative – Magnesium

A biocompatible metal that has similar mechanical properties to human bone is required to prevent stress shielding. Magnesium alloys have mechanical and physical properties, such as elastic modulus and density, that are more similar to those of natural human bone as compared to traditional bio-metals [5] (Table 1).

Moreover, magnesium alloys have a moderate degradation rate to comply with the fracture-healing processes and good non-toxicity of degradation products. In addition, magnesium is an essential element of the human body and helps in regeneration of natural bone [6, 7]. The human body can accommodate Mg ions released due to

degradation of an implant, and the excess ions can be successfully excreted. Hence, magnesium alloys are a suitable candidate for implant materials.

Table 1: Physical and mechanical properties of human bone and implant alloys [5]

Properties	Bone	Mg	Ti	Co-Cr	SS
Density (g/cm^3)	1.8-2.1	1.7-2.0	4.4-4.5	8.3-9.2	7.9-8.1
Elastic modulus (GPa)	3-20	41-45	110-117	230	189-205
Comp. yield strength (MPa)	130-180	65-100	758-1117	450-1000	170-310
K_{IC} (MPa·m$^{1/2}$)	3-6	15-40	55-115	N/A	50-200

1.1.4 Corrosion Mechanism of Magnesium – Electrochemistry

Corrosion is defined as the destruction or deterioration of a material because of reaction with its environment under the influence of chemical, physical, and electrochemical factors [8]. Corrosion of a metal in the physiological environment is more complicated than corrosion in natural scenarios due to the effect of protein and changing pH.

During corrosion of magnesium (Mg), metallic Mg is converted to a stable Mg^{+2} ion in two electrochemical steps [9]. The first step involves conversion of Mg to a uni-positive Mg^{+} ion, as an intermediate reaction, equations (1) and (2).

Anodic reaction:

$$Mg \rightarrow Mg^{+} + e^{-} \quad (1.1)$$

$$k Mg^{+} \rightarrow k Mg^{2+} + k e^{-} \quad (1.2)$$

Anodic reactions

where, k = a fraction of uni-positive Mg^{+}

These partial reactions are balanced by cathodic partial reactions of hydrogen evolution:

Cathodic reaction:

$$(1+k)H_2O + (1+k)e^- \rightarrow \tfrac{1}{2}(1+k)H_2 + (1+k)OH^- \quad (1.3)$$

As Mg^+ can chemically react with water, a fraction of Mg^+ reacts electrochemically via Eqn. 1.2. The complement of Eqn 1.2 reacts with water as:

$$(1-k)Mg^+ + (1-k)H_2O + (1-k)OH^- \rightarrow (1-k)Mg(OH)_2 + \tfrac{1}{2}(1-k)H_2 \quad (1.4)$$

Overall reaction is given as:

$$Mg + 2H_2O \rightarrow Mg(OH)_2 + H_2 \quad (1.5)$$

Hence, the corrosion of magnesium is only partly electrochemical. The predicted corrosion rate by electrochemical measurements is expected to be lower than the real corrosion rate (as determined by the hydrogen evolution or the weight loss method) [9].

1.1.5 Corrosion Mechanism of Magnesium in a Physiological Environment

Magnesium is oxidized immediately after coming in contact with body fluids to form metal cations as seen in equations 1.1 and 1.2. The released electrons are consumed by water molecules resulting in a water reduction cathodic reaction (Eqn. 1.3) [9]. These reactions happen over the exposed surface of an implant material, where a galvanic cell is formed due to potential difference between the metal and its grain boundaries. At the same time, organic molecules (such as proteins, amino acids and lipids) get adsorbed on the metal surface, thus leading to the dissolution of metal. A corrosion layer of the

product formed (magnesium oxide) is accumulated on the surface as shown by Eqn. 1.5. As the implantation time increases, cells are observed to adhere and proliferate on the metal surface, which leads to a natural tissue formation. The product layer later breaks down into several small particles and is further degraded by tissue.

1.1.6 Biosafety and Disposal of Degraded Products

The local physiological and chemical equilibrium is often disturbed due to the generated corrosion products at the implant contact site. The effect of this interaction gives rise to metal cations (as indicated in equations 1.1 to 1.5), chemical products (such as oxides, hydroxides, phosphates, carbonates from body fluids), local change in pH, and release of hydrogen gas (Eqn. 1.5). Magnesium degradation is safe and harmless to the body only when the concentration of these products is under a certain range [10]. For instance, higher corrosion rate of magnesium alloy can give rise to higher amounts of hydrogen gas evolved per interval of time. Gas cavities can be produced in the tissue surrounding the implant and can gradually diffuse in the extracellular mediums that keep circulating depending on the local blood flow [3]. However, gas cavities were not observed in the case of coated magnesium alloys, as they exhibit lower initial corrosion rates as compared to bare magnesium alloys.

(a) Precipitate disposal

The precipitates of metal oxides disintegrated through the degradation process show relatively low solubility in body fluids and are difficult to eliminate from the body. However, the most common by-product of magnesium degradation is magnesium

hydroxide ($Mg(OH)_2$), which reacts with chloride ions from body fluids to form soluble magnesium chloride ($MgCl_2$) [11, 12].

(b) Toxicology

The released products can induce system toxicity and/or local toxicity to the human body. If the alloy degrades too fast, the local pH value can elevate too fast, thus causing toxicity in peri-implant cells and local tissues with an increase in the inflammatory response. Although magnesium alloys have shown affirmative results in terms of biocompatibility on animal models, several flaws such as formation of gas cavities (due to rapid degradation of alloys) and severe hemolysis (due to drastic increase in pH values) have also been observed [13].

1.1.7 Corrosion Challenges for Magnesium

The *in vitro* tests for Mg are classified into two broad categories: i) corrosion resistance and ii) toxicity. In most cases, both categories are related to each other due to rapid degradation that can lead to many biological reactions [14]. Hence, the major challenge of using magnesium alloys as implants is to decrease their degradation rate in physiological conditions. The critical technical obstacle is to understand how to improve the corrosion resistance of magnesium.

1.1.8 Methods to Improve Corrosion Resistance of Magnesium

Improving corrosion resistance is essential for manufacturing a favorable implant. Different methods to slow corrosion include alloying, coatings, and surface treatments.

(a) Alloying

Alloying elements associated with improving corrosion resistance include: i) aluminum (Al) and zirconium (Zr) in ingot alloys and ii) passivating elements such as nickel (Ni) and rare earth elements (*e.g.*, yttrium (Y) and neodymium (Nd)) in amorphous alloys [15]. The benefits of using these alloying elements include improving the protective properties of a surface film.

(b) Coatings

A coating on magnesium alloys is one of the most popular methods used in order to improve corrosion resistance [8]. The coating is required to have sufficient adhesion on metal surfaces; resistance to corrosion, wear and fatigue; and high hardness and mechanical strength. So far there are no coatings that satisfy all the demands. The selection is made based on type of implant or application. Metal coatings (such as electroless nickel plating, chromate conversion coating, or aluminum coating) have high hardness and good mechanical properties, but they are toxic to the human body. However, non-metal coatings (such as thermal spray coating or anodizing) have low strength and wear resistance.

(c) Surface Treatments

Surface treatments such as laser shock peening, shot peening, and roller burnishing are used to influence the mechanical properties of the implant material. The residual compressive stresses induced by these treatments can improve fatigue life and

corrosion resistance. Furthermore, surface treatments are beneficial for tissue growth due to surface modification. However, the effect of stress-corrosion and corrosion-fatigue behavior of these surface treated alloys is unknown. Hence, it is important to investigate the effects of surface treatments for considering their application in orthopedics.

1.1.9 Types of Mechanical Surface Treatments

(a) Laser Shock Peening

Laser shock peening (LSP) is a non-contacting surface treatment that causes plastic deformation of a workpiece via shock pressure wave loading [16]. LSP induces compressive residual stresses in the alloy by generating a high strength impact wave. LSP improves the mechanical properties to control the implant's corrosion rate, and provides suitable surface for cell attachment on the implant [17].

(b) Burnishing

Burnishing is a contacting surface treatment that causes plastic deformation of a metal via a hydrodynamic ball that applies a force in rolling/sliding contact [18]. The force applied in this type of rolling/sliding contact induces compressive residual stresses near the surface of the metal alloy.

(c) Shot Peening

Shot peening (SP) is a contacting surface treatment where metal/ceramic/glass media is shot at high velocity to deform the surface of the metal alloy [18]. The plastic deformation by shot peening induces deep compressive residual stresses below the

surface. The process of spraying media results in a random distribution of pits that leads to increase in surface roughness.

1.1.10 Why Shot Peening?

While all the above-mentioned surface treatments are beneficial in their own way, selection of a surface treatment needs to be done based on the geometry and application of the implant. Burnishing gives a smooth surface as compared to SP and LSP, and hence it may not create the required surface for the cell attachment. LSP is an expensive localized surface treatment. Shot peening can be applied to large areas economically while simultaneously providing a rough surface; thus, SP is well suited for the face of a large bone plate.

1.1.11 Cell Behavior on Magnesium Implants

Most of the currently used commercial orthopedic implants are coated with different materials. The cell viability on the surface is difficult to understand if there is a crack in the coating or once the coating is degraded. Similarly, it is essential to understand the cell behavior on surface treated implants. As magnesium is a degradable material, the surface of an implant slowly degrades inside the human body. The residual stresses subject to the surface at a given time will be different. Thus, it is essential to consider the effect of degrading surface on the cell behavior.

At the same time, surface treatments create a unique roughness on the surface an alloy. It is difficult to evaluate the cell attachment and proliferation with surface roughness as a changing parameter. Ultimately, it is required to find out how residual

stresses from a surface treatment affect cell attachment, proliferation, and viability on a degrading and rough surface.

1.2 Research Objectives

Shot peening process has been used to modify the surface integrity of magnesium alloy (WE43). The objective of this study is to understand the effect of shot peening on the stress corrosion behavior of WE43. The focus of this research is the following: (1) measure the surface integrity imparted by the shot peening process; (2) understand corrosion behavior of the alloy when the specimen is stressed and unstressed; and (3) find a relation between SP process parameters, surface integrity, and the stress-corrosion behavior of the alloy.

CHAPTER 2

STRESS-CORROSION OF MAGNESIUM ALLOYS

2.1 Magnesium Alloys as Orthopedic Implants

As technology progresses, several materials are considered for implantation during an orthopedic surgery. Applications include scaffolds for osteogenesis or fixtures for supporting a fractured bone. The material needs to be biocompatible for it to be suitable in various surgical applications. Currently, different materials such as stainless steel, cobalt-chromium, titanium alloys, and various ceramics and polymers are used to serve this purpose. Since these materials are not biodegradable and have high (metals) or low (polymers) strength as compared to the human bone, several problems and complications arise from long-term implantation that limits their utility [19]. An alternative biomaterial that avoids long-term complications since it fully degrades is magnesium. Magnesium alloys possess several benefits that make them of interest for orthopedic applications. They have mechanical properties similar to that of human bone, which helps avoid stress shielding. Also, magnesium corrosion products safely exit the body through normal metabolic activity. The biocompatible nature of magnesium and the similar properties to bone make it an ideal material for biodegradable implants.

2.1.1 Recent Development of Magnesium Alloys as Orthopedic Implants

Some of the magnesium biomedical device products manufactured currently include scaffolds, stents, bone pins and screws. Researchers at the Fraunhofer Institute of Laser Technology have developed a selective laser melting process to manufacture

complex structures of implants for different materials, including magnesium alloys (Figure 2.1(a)) [20]. The biocompatibility of these magnesium implant prototypes has been demonstrated *in vitro*.

Magnesium Elektron and Biotronik have partnered to develop a cardiovascular stent that resorbs over time (Figure 2.1(b)). In 2016, a new product called *Magmaris magnesium scaffold* was launched and it is the world's first clinically approved magnesium-based resorbable scaffold to obtain a CE mark [21].

Syntellix (Hannover, Germany) developed a MAGNEZIX compression screw and demonstrated good biocompatibility and osteoconductive quality *in vivo*. MAGNEZIX is an aluminum-free magnesium alloy and belongs to MgYREZr alloy group, that is similar to WE43 (Figure 2.1(d)) [22].

U&I Corporation (South Korea) manufactures headless and cortex screws, and K-wires with Mg-Ca alloy that completely degrade in 6 to 18 months depending on implant application. U&I's alloy has proven biocompatibility (ISO 10993) and produces no stress shielding [23].

nanoMAG produces several innovative devices including bioabsorbable devices (orthopedic fixation devices for spine, hip, and femur trauma) and biomedical external devices (light weight knee, foot, and elbow braces) made of magnesium. They have proved biocompatibility *in vivo* (Figure 2.1(c)) [24].

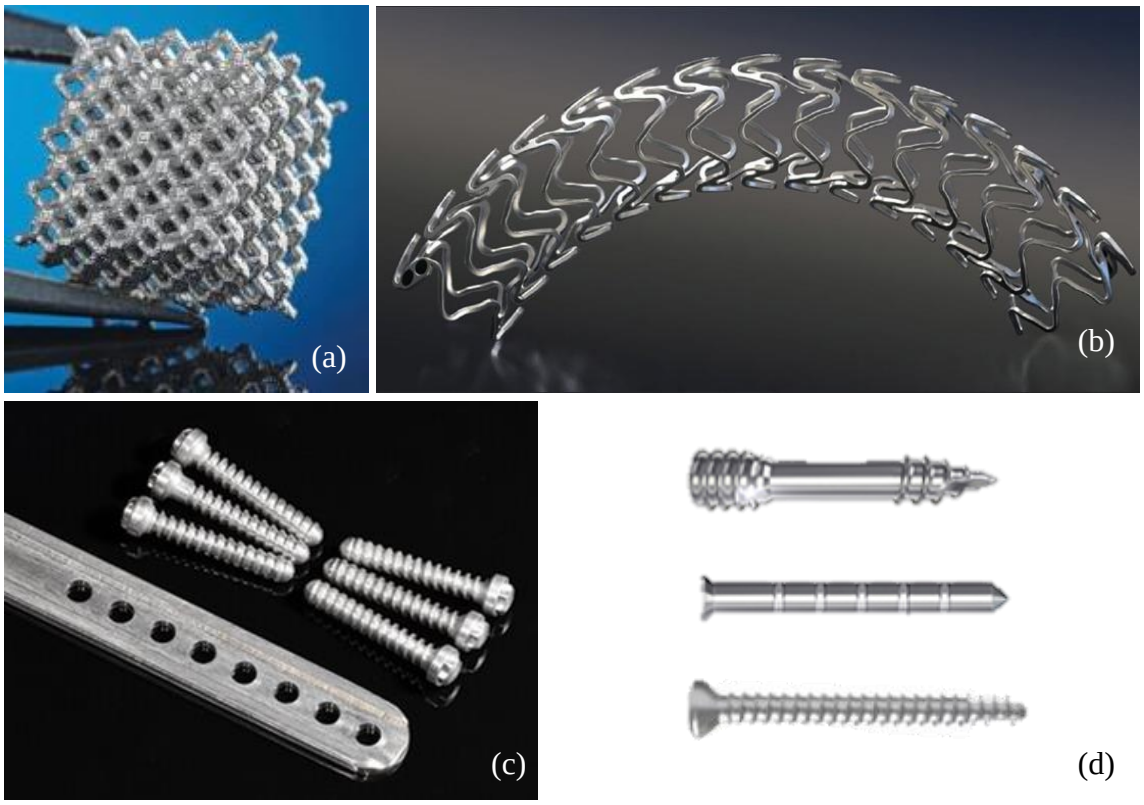

Fig. 2.1: (a) Scaffold with defined pore structure made from WE43 (Fraunhofer, Aachen), (b) stent created by Biotronik using magnesium alloy, (c) fracture fixation magnesium plates and screws developed by nanoMAG, (d) bone screws and pins made of magnesium alloys and developed and manufactured by Syntellix.

2.1.2 Competition with Biodegradable Polymers and Permanent Metallic Materials

There are many biodegradable polymers such as LPLA, DLPLA, PGA and PCL that have been approved by the FDA. These polymers are used in fracture fixation surgeries as pins, plates, interference screws, suture anchors, *etc*. Polymeric devices are vastly used in low to mild load bearing applications. However, biodegradable metals like magnesium are viewed as the promising alternatives to polymeric devices in hard tissue repair.

In comparison with permanent metal materials such as Ti, Co-Cr, and stainless steel alloys, biodegradable metals have shown encouraging results in hard and soft tissue

applications. Improving the mechanical properties and better predicting the degradation behavior will broaden the use of biodegradable metals in orthopedic applications.

Overall, the competition of biodegradable alloys with permanent metal alloys and polymer devices is relatively low at this stage of development. It is predicted that the competition will be relatively higher in future years with progress in research [25].

2.1.3 Corrosion of Magnesium Alloys

Magnesium is a highly active metal and is prone to corrosion in slightly alkaline solutions. The Pourbaix diagram of magnesium in water at 25°C is shown in Figure 2.2. The regions of corrosion, passivation, and immunity according to their pH are indicated in the diagram. The diagram indicates that magnesium is passive in highly alkaline solutions, *i.e.*, with a pH of 12 or higher. The pH of human body remains in the range of 7 to 8.4. Thus, for corrosion testing of magnesium for biomedical applications, the pH is maintained in the same range to make sure that magnesium does not enter passivation mode. The corrosion reactions of magnesium have been explained in Chapter 1, Section 1.1.3.

2.1.4 Corrosion Rate of Magnesium

The major challenge for magnesium implants is high corrosion or degradation rate. Rapid corrosion of magnesium affects the mechanical stability of the implant. The corrosion products can accumulate in the body and can lead to rapid pH change of the body. To avoid these drawbacks, it is important to control the corrosion rate of magnesium.

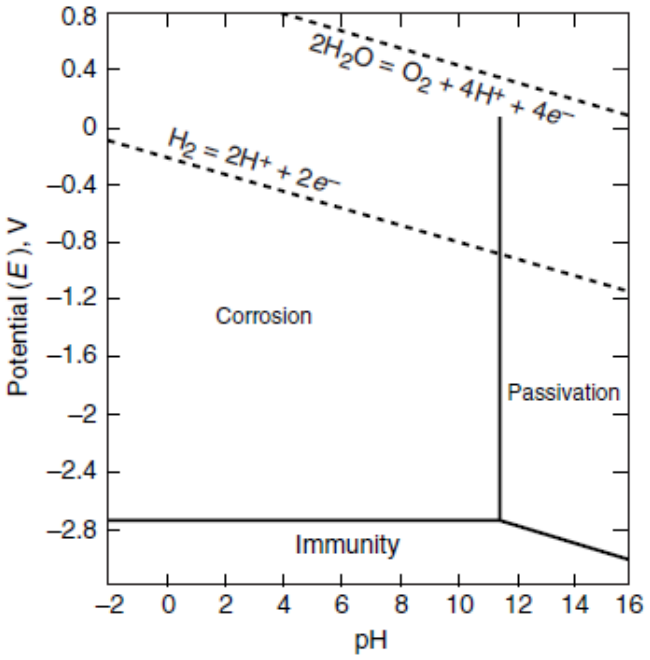

Fig. 2.2 Pourbaix diagram of magnesium in water at 25°C.

2.1.5 Influencing Corrosion Behavior of Biodegradable Magnesium

(a) Alloying

The degradation rate of pure magnesium is extremely high and needs to be controlled in order to avoid the harmful effects to the human body. Alloying is a good solution to improve corrosion resistance of high purity magnesium. Alloying elements in their pure form or intermetallic phase are used to make magnesium more noble. Alloying elements such as aluminum, manganese, calcium, lithium, rare earth elements are currently used to control the degradation rate [26].

From a biocompatibility point of view, there are not many elements suitable for alloying magnesium. Each element associated with magnesium alloying comes with its own advantages and disadvantages. Aluminum (Al) can provide strength to the implant, but Al ions can react with inorganic phosphates thus inducing dementia in the human

body. Rare earth elements (such as Ce, La, Nd, and Pr) are used to improve hardness of the alloy, but some of those elements (Pr, Ce, and Lu) can exhibit toxicity to the body. Zirconium is used as a grain refiner and to avoid aluminum in the alloy. It has been found that liver, lung, and breast cancer are closely related with presence of zirconium [27].

(b) Coatings

A suitable corrosion resistant coating can delay the initiation of degradation of magnesium. A delay in degradation is required as the implant needs to function properly for a certain duration after the surgery and before the tissue starts to heal. The coating should also be wear resistant, as it should not get damaged during implantation. A non-toxic anodized coating, similar to a ceramic was produced and tested in a lab [27]. Results indicated there was no hydrogen evolution in the physiological solution for a month. Thus, anodized coating successfully delayed the biodegradation of commercial purity magnesium (CP-Mg).

If the coating breaks down, the anodized coating is non-toxic and silicon oxides from the coating dissolve into the body fluids. The degradation of magnesium starts occurring at the break-down area. Thus, the coverage and thickness of coating can be varied according to the preferred degradation area and degradation rate can be controlled accordingly [27].

(c) Surface Treatments

Low fatigue strength and low corrosion resistance are some of the factors that negatively influence the ease of using magnesium as orthopedic implants. Mechanical

surface treatments such as shot-peening, roller-burnishing, laser shock peening, and deep-rolling are performed on magnesium alloys to improve corrosion and fatigue performance [28].

Laser shock peening (LSP) is a surface treatment method to impart high compressive residual stresses in magnesium alloys. Effect of LSP on corrosion resistance of Mg-Ca alloy was studied by Sealy *et al.* [29, 30]. The references [17, 31, 32] discuss the effect of high-repetition rate laser shock peening on biodegradable magnesium.

Shot peening has been initiated and its effect on corrosion resistance of magnesium alloys such as AZ80, AE21 and AZ31 has been discussed in [33-35]. Ultra-fine burnishing is used to control corrosion rate of Mg-Al-Zn alloy [36] and AZ31 alloy [37]. Effect of other surface treatments such as plasma vapor deposition (PVD) on corrosion resistance of magnesium alloys have been studied [38, 39]. Figure 2.3 indicates the list of all treatments/modifications that can be done to improve corrosion resistance of magnesium.

2.2 Stress Corrosion Cracking

Stress corrosion cracking (SCC) is a dangerous and complicated form of corrosion that involves a three-way interaction: (*i*) mechanical loading, (*ii*) a susceptible environment, and (*iii*) a corrosive environment [41].

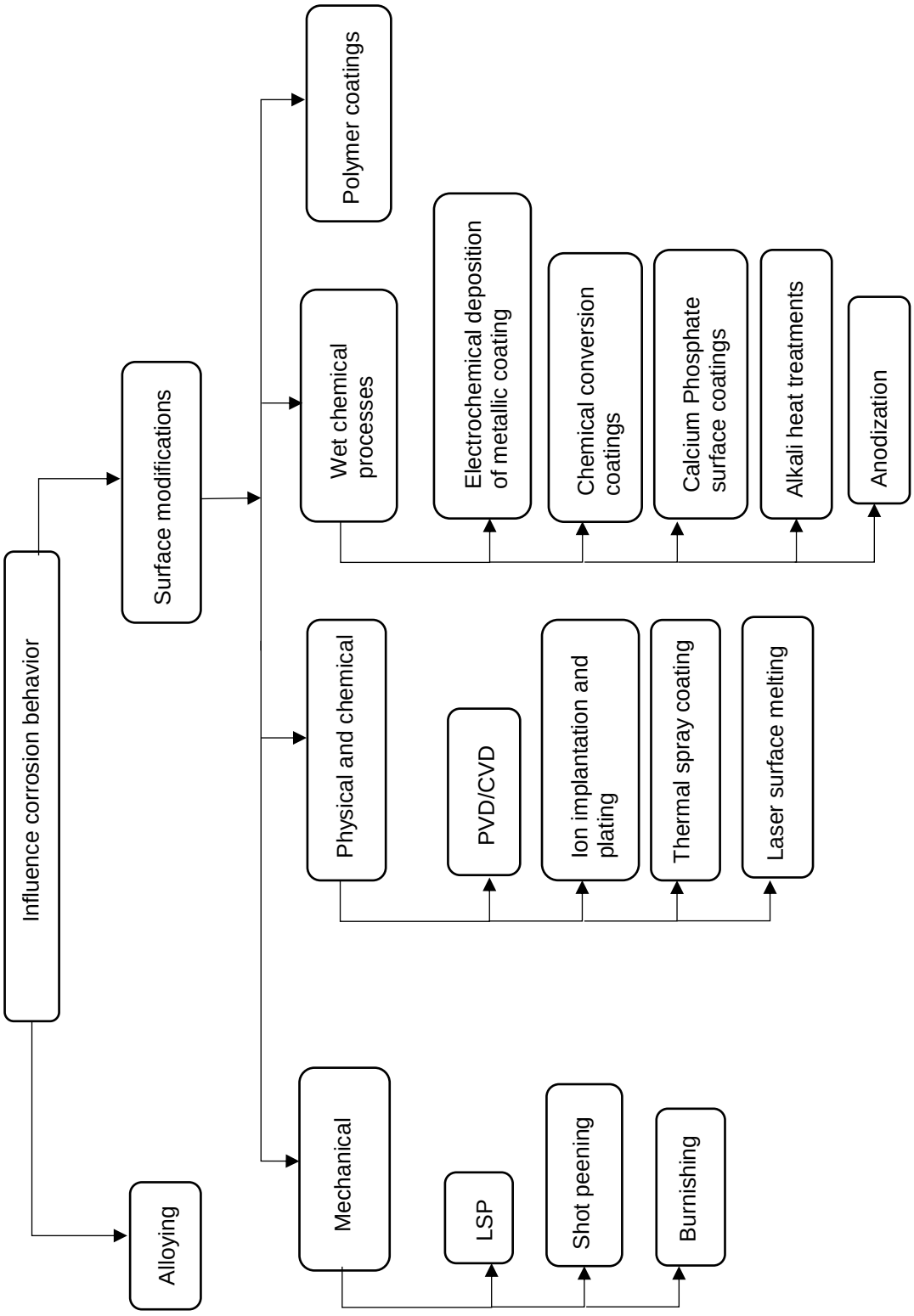

Fig. 2.3 Methods to influence corrosion behavior [40].

2.2.1 SCC Mechanism

An increase in the chemical activity is observed when an electrochemical potential difference is formed between stressed and unstressed parts of a metal. Such kind of stress-initiated corrosion mechanism usually accelerates the corrosion rate by two to three times the normal uniform rate. This results in formation of small cracks that concentrate stress within the loaded implant. Stress corrosion cracking can occur in any stress loaded implant immersed in aqueous solution of body fluids. The cracks generated by SCC extend rapidly and grow in between grain boundaries of the stress affected region. The crack speed is dependent on the strain rate from implant loading cycle and the presence of hydrogen gas produced by corrosion reaction [40].

2.2.2 Metallurgical Effects

Magnesium alloys show poor corrosion resistance, even in dilute electrolyte solutions. Detection of stress corrosion cracking is difficult, although significant microstructure changes occur. Studies have been done to identify the effect of stress corrosion cracking on the microstructure of magnesium by different methods. Investigation of stress corrosion cracking in WE43 magnesium alloy has been done by using quantitative fractography methods [42]. A strain rate of 9.10^{-7} s^{-1} was applied to cylindrical samples of 5 mm diameter and 20 mm length, along with corrosive environment exposure for 73 hours. Many SEM images were merged together to form a high-resolution fracture micrograph after exposure. The micrograph was then provided as an input to quantitative fractography. A manual detection using the GIMP software gave the following results (Figure 2.4):

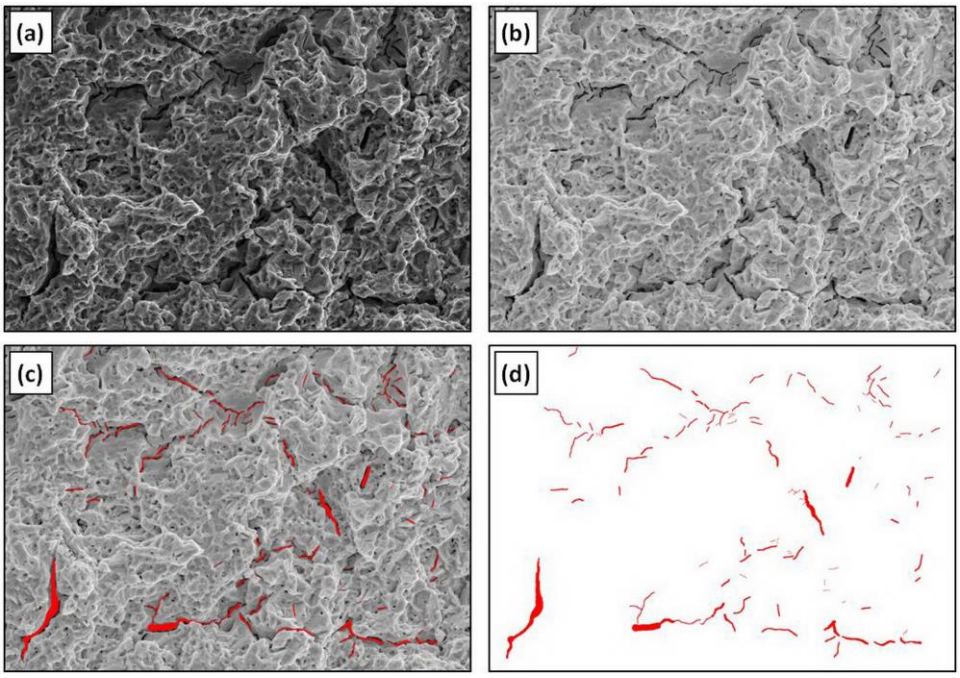

Fig. 2.4 Detection of cracks due to SCC of WE43 [42].

2.2.3 Electrochemical Effects

Various experiments have been conducted to determine the effect of stress corrosion on the electrochemical properties of magnesium alloys. A study by Yu *et al.* [43] reported the results at low strain rates. Stress corrosion cracking of Mg-Zn-In-Sn alloy in 3.5% NaCl solution at 25°C was observed under an optical microscope. The electrochemical measurements of open circuit potential (OCP) and loop circuit (LC) were taken with a potentiostat. It was observed that the stability of OCP was improved with increase in stress (in elastic region). At the same time, the LC values of alloy improved with increase in stress in elastic zone. The effect of SCC on the electrochemical properties of Mg-Zn-Y-Zr alloy was also reported by Wang *et al.* [44].

2.2.4 Methods of Prevention of Stress Corrosion Cracking

The prevention of SCC depends on several different factors. The general principle to prevent SCC is to avoid loading the alloy above the critical stress while exposed to corrosive environment. However, it is difficult to stay within the limits of critical stress in applications such as biomedicine. There are a few guidelines to follow when it comes to engineering materials that are subjected to stress and corrosion at the same time [41].

- Conception and design: Engineering a part such that there is less concentration of stresses at the start, during the use, or through increasing susceptibility to degradation. Avoiding complex geometrical aspects to the part can prevent SCC
- Service environment: Keeping dry atmosphere with the relative humidity less than 95% can lower the risks of stress corrosion cracking
- Alloy selection: Selecting an appropriate alloy + environment combination for a particular application helps avoid SCC
- Service loading: The total stress during use (service stress + fabrication stress + residual stress) should be lower than the threshold stress (50% of yield stress)

2.2.5 Mechanisms of Stress Corrosion Cracking

Numerous mechanisms of stress corrosion cracking have been proposed through an extensive experimental investigation and theoretical analysis. Mechanisms that have received greatest attention have been discussed briefly in the following sections.

(a) Hydrogen Embrittlement

Hydrogen induced cracking, a mechanism that has brittle cleavage-like features, accounts for stress corrosion cracking. The interatomic bonds of the material are weakened by hydrogen atoms in the plane strain region at the crack tip (Figure 2.5(a)). The result is a singular crack with branching.

(b) Adsorption Induced Cleavage

The critical anions from the solution are adsorbed during the electrochemical process. The metal bonds at the crack tip are weakened by these anions and a crack is initiated (Figure 2.5(b)). The crack grows until it is blunted by plastic deformation or grows out of the adsorbed region.

(c) Atomic Surface Mobility

In atomic surface mobility mechanism, the crack grows by the capture of surface vacancies at the crack tip and counter-current surface diffusion of atoms away from the crack tip (Figure 2.5(c)). There is not a lot of support for this mechanism at present.

(d) Film Rupture

Film rupture or slip-step dissolution is one of the first proposed SCC mechanisms and still receives considerable support. Tensile stress produces strain to rupture the surface film at an emerging slip band [45]. A crack grows at the rupture site by anodic dissolution of the bare surface (Figure 2.5(d)). The crack grows until the crack tip can re-passivate or grow until failure.

(e) Film-Induced Cleavage

Brittle films are present on the surface of several metals. This mechanism postulates that a crack growing in the surface film may propagate further into underlying metals if it reaches sufficient velocity at the interface (Figure 2.5(e)). Corrosion is necessary to form surface films, and not propagate cracks. Reformation of surface film is required at the crack tip surface before a new crack is formed.

(f) Localized Surface Plasticity

This mechanism proposes that stress corrosion cracking results from a defect structure ahead of the crack tip that produces plasticity (Figure 2.5(f)). This could result in formation of localized critical corrosion effect.

2.3 Stress Corrosion Cracking of Magnesium for Biodegradable Implants

2.3.1 How does SCC relate to Biodegradable Implants?

A biodegradable implant is subjected to many tensile and compressive stresses arising from different activities (such as lifting objects, walking, *etc*.) in a human body. It is also exposed to body fluids to begin the degradation process. Thus, the conditions required for initiation of SCC such as susceptible metal alloy (biodegradable implant), corrosive environment (body fluids), and application of stress (through various movements of the body part) are fulfilled. It is required to study and understand the stress corrosion behavior of the material to develop a favorable orthopedic implant.

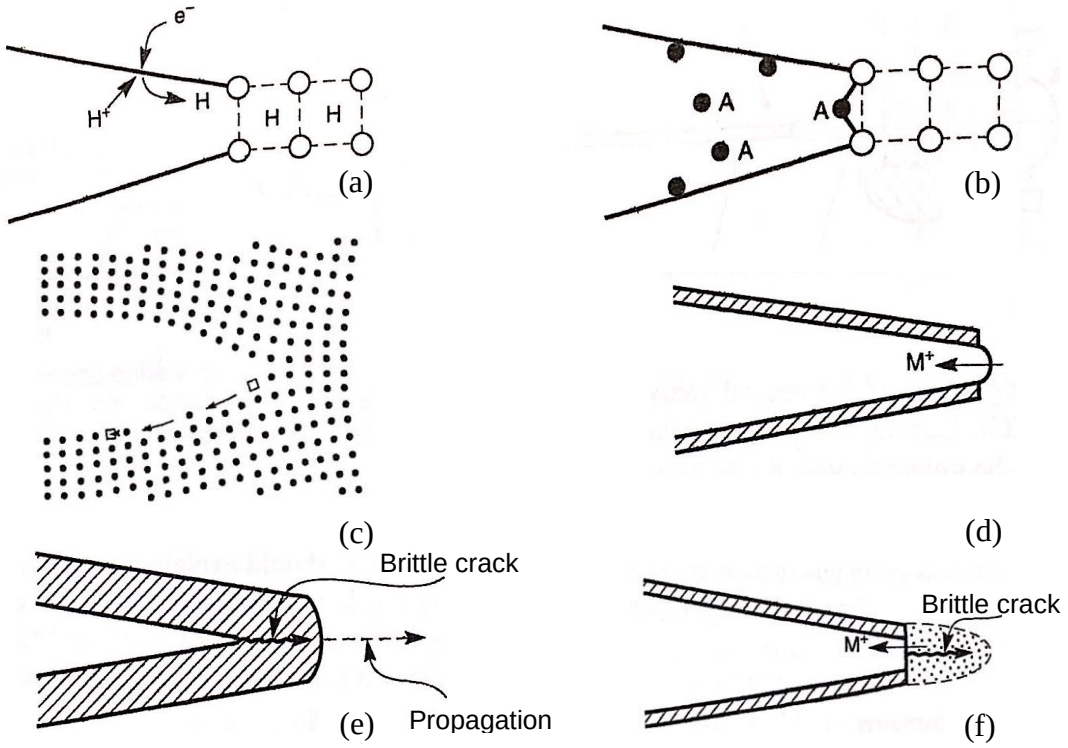

Fig. 2.5 Mechanisms of stress corrosion cracking growth: (a) hydrogen embrittlement, (b) absorption induced cleavage, (c) surface mobility, (d) film rupture, (e) film induced cleavage, and (f) localized surface plasticity [45].

2.3.2 Stress-Corrosion Environment In-Vivo

A biomedical implant is often subjected to stresses depending on the human body part where the implantation is done. For example, a femur plate can experience 3 to 4 times a patient's body weight after implantation. Due to these stresses, and by the principles of SCC, the implant degrades rapidly. Moreover, the human body fluids are salt-based solutions that accelerate corrosion. Hence, the composition of body fluids account for stress corrosion cracking behavior. Magnesium alloys have been tested *in vivo* [4]. Various alloys such as AZ31, AZ91, WE43 have been tested on animal models using ISO standards. Different problems related to these alloys have been discussed in [4].

2.3.3 Effect of Magnesium Metallurgy on SCC

(a) Microstructure

The effect of microstructure on SCC of Mg-Al-Zn alloys has been observed in [46]. Results indicate that a large size and spacing of grain boundary precipitates decrease the degradation rate. The effect of microstructure on SCC behavior of Mg-xSn alloys was observed in [47]. The morphology changed from spherical to a semi-continuous network as the concentration of added Sn was increased from 2% to 8%. Higher concentration of Sn diminished the SCC resistance. These studies indicate microstructure plays an important role in the SCC behavior and is highly dependent on the alloy composition.

(b) Alloying

The SCC susceptibility for alloys with different element combinations is different. The SCC tendency of some common magnesium alloys is given in (Table 2 of [41]). The SCC resistance to different environment combinations is given in (Table 3 of [41]). The measure of SCC susceptibility is SCC threshold, K_{ISCC} or σ_{SCC}. For example, SCC susceptibility was reported to increase by 6% with addition of aluminum. Addition of Nd, Zr, Pb, Cu, and Ni had little or no influence on SCC [41].

2.3.4 Gaps in the Literature

Although it is hypothesized that coatings and surface treatments affect SCC of magnesium alloys, there was no literature explicitly investigating these topics and is a prime motivation for the proposed study. Surface treatments are of particular interest for this work. Surface treatments are well known to impart favorable surface integrity's that

affect corrosion behavior. The primary mechanism believed to influence SCC is localized surface plasticity. This work is an initial study in the field and will help identify shot peening's influence on SCC.

2.3.5 Methods to Measure Stress Corrosion Cracking

The following three parameters are considered to characterize SCC:

- threshold stress, σ_{SCC}
- threshold stress intensity factor, K_{ISCC}
- steady stress corrosion crack velocity, V

There is no general approach to predict SCC based on micromechanics and physical metallurgy. Stress corrosion cracks are macroscopically brittle, although local plasticity is required for the crack to proceed. Hence, linear elastic fracture mechanics (LEFM) is used to measure SCC. The stress intensity factor (K_I) at the crack tip is given by:

$$K_I = Y\sigma\sqrt{\pi a} \tag{2.1}$$

where Y is a geometric factor, σ is applied stress, and *a* is crack length. The effect of the K_I on crack velocity varies for different alloys in different environments. A detailed list of different alloys and their crack velocities has been mentioned in [41].

2.4 Modeling Stress Corrosion Cracking using Peridynamics

2.4.1 Introduction to Peridynamics:

Peridynamics, a reformulation of the classical continuum mechanics, allows for a natural treatment of discontinuities in materials by employing the concept of nonlocal

interactions [48]. This method can be used to simulate several complicated problems. According to continuum mechanics, a material point can interact with material points that lie in its direct contact, or nearest neighborhood (Figure 2.6) While classical continuum mechanics has been used to solve various problems in engineering, it cannot be used for parts with discontinuities. The governing equations in continuum mechanics are partial differential equations. When a discontinuity like a crack or geometrical part void is observed, the spatial derivatives are not defined and the solution attains singularity [49].

To overcome this drawback, a non-local continuum mechanics formulation was introduced by Silling [50] such that all the discrepancies for modeling objects with discontinuities were solved. In this method, a material point can interact with material points within a defined neighborhood, called horizon (H_x, radius δ) (Figure 2.6). The governing equation of peridynamics is given as:

$$\rho(x)\ddot{u}(x,t) = \int_{Hx} f(u(x',t) - u(x,t), x' - x)dV_{x'} + b(x,t) \qquad (2.2)$$

where ρ, u, and $\ddot{u}$ represent density, acceleration, and displacement of the material. The variable $b(x,t)$ represents body forces acting on the material point x at time t. This integro-differential equation leads to non-singular stresses, and is mathematically consistent regardless of any discontinuities present in the domain, like cracks.

2.4.2 How does Peridynamics relate to Mg Corrosion?

Peridynamics can be used in various applications to simulate fracture, impact, corrosion rate, heat transfer, advection, diffusion, *etc*. A peridynamic model to

understand damage from pitting corrosion was developed by Bobaru *et al.* [51, 52]. The anodic reaction in corrosion process was modeled as a peridynamic diffusion process in metal-electrolyte coupled system. Thus, the autonomous evolution of metal-electrolyte interface was identified to evaluate sub-surface damage.

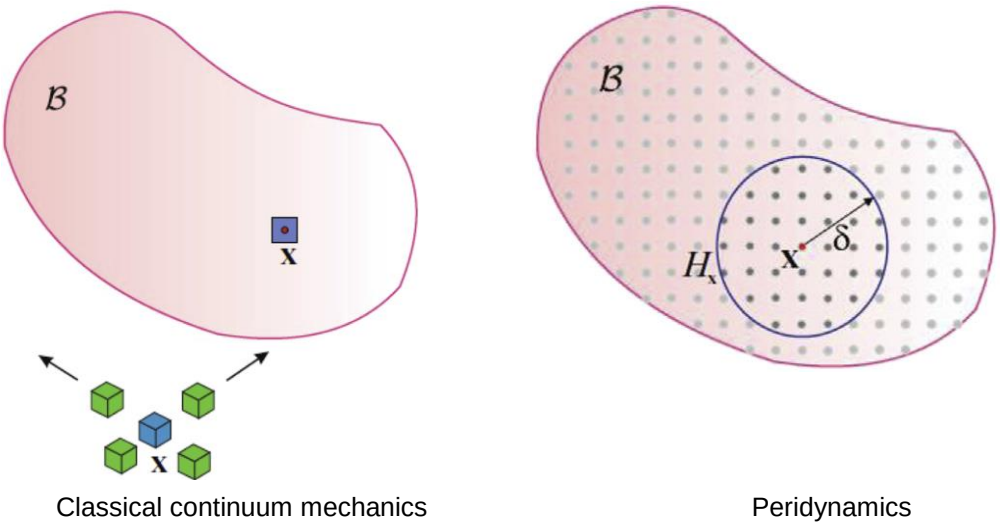

Fig. 2.6 Interaction of a material point in continuum mechanics and peridynamics.

The peridynamic modelling of adsorbed-hydrogen stress-corrosion cracking was done based on the adsorption-induced decohesion mechanism by Meo *et al.* [49]. The mechanical behavior of the material was found using microstructure data.

The effect of stress-corrosion on the strength of a ZK60A Mg alloy was studied by Bobaru *et al.* [48]. The corrosion process can lead to development of cracks in the high stress regions. It was observed that ductility of this alloy was reduced after corrosion due to the microstructural properties of the diffusion corrosion layer (partially oxidized layer).

Identification of stress-corrosion rate is important when it comes to biomedical implants. The stress-corrosion behavior of an implant changes according to a patient's age and weight. Moreover, it is difficult to predict the corrosion rate of implants with complicated geometry, such as a femur. Hence, it is essential to model stress-corrosion behavior of a customized implant. Peridynamics can be effectively used to predict the failure or behavior of a biomedical implant. The material model in the peridynamic code can also accommodate the properties of the implant material.

CHAPTER 3

SHOT PEENING OF MAGNESIUM ALLOYS AND SURFACE INTEGRITY CHARACTERIZATION

3.1 Research Objectives

The aim of this study is to understand how shot peening (SP) process parameters affect part performance by influencing surface integrity. The relation between SP process parameters, surface integrity, and part performance is indicated in Figure 3.1. By finding an optimal relationship between these three categories, a favorable implant can be manufactured according to a patient's age and weight. This chapter will discuss the first two criteria: SP process parameters and surface integrity of magnesium WE43.

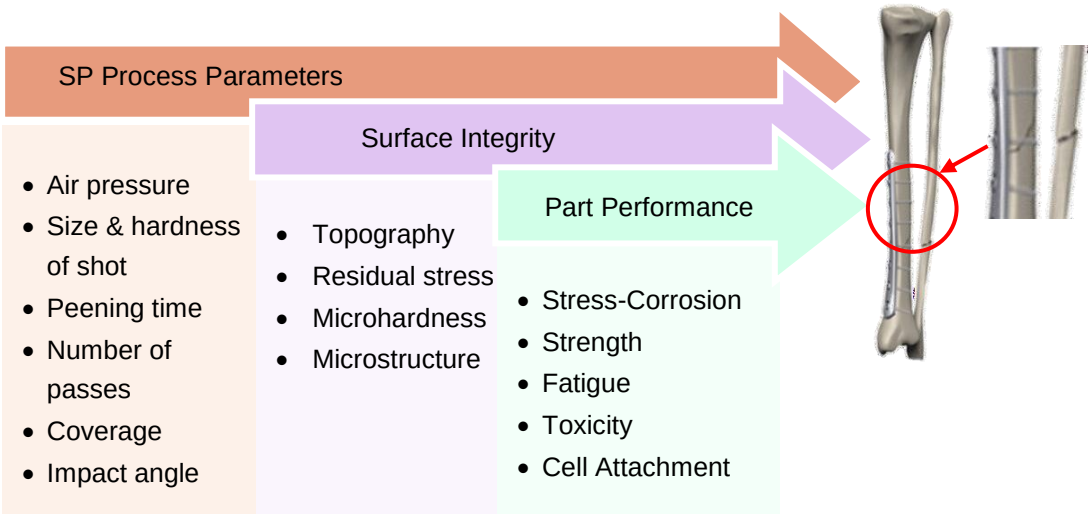

Fig. 3.1 Schematic showing the relationship between some SP process parameters, surface integrity, and performance of degradable implant. Modified from [53].

3.2 Shot Peening

3.2.1 Definition: Shot Peening

Shot peening is a cold working process in which the surface of a part is bombarded with small spherical media called shot [54]. Each particle of spherical media acts as a tiny peening hammer and strikes the material, thus creating several small indentations/dimples on the surface of the material (Figure 3.2). The surface undergoes tension due to the formation of indentations. The material just under the surface tries to restore its original shape by maintaining high compression stresses. An even layer of compressive residual stresses is formed due to the overlapping of dimples.

Shot peening increases resistance to fatigue failure, stress corrosion cracking, corrosion fatigue, intergranular corrosion, hydrogen-assisted cracking, *etc*. Apart from work hardening, other benefits or applications of shot peening include surface texturing and testing the bond of coatings.

3.2.2 Residual Stresses

Residual stresses are those stresses remaining in a part after all manufacturing operations are completed, with no external load applied [54]. They can be tensile or compressive in nature. For example, in a welded joint, the heat-affected region near the weld may have tensile residual stresses. Induction-hardened or surface-treated parts may have compressive residual stresses. The maximum compressive stresses induced due to shot peening are approximately half the yield strength of the shot peened material.

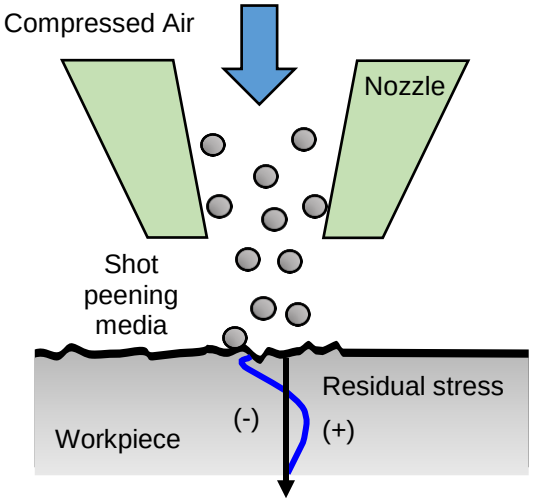

Fig 3.2 Schematic diagram of shot peening process.

3.2.3 Process Variables

To maintain the repeatability and preciseness of the process, all process variables need to be identified and controlled [2]. Some of the fundamental factors affecting the shot peening process are:

- Shot density
- Size and hardness of shot
- Nozzle diameter and length
- Air pressure
- Impact angle
- Distance between nozzle and workpiece

Shot density (also known as coverage density or coverage) refers to the percentage of the surface indented and is usually monitored by visual inspection. Some primary factors affecting shot density are the material flow rate, exposure area and time, and shot properties (size, composition, hardness). Coverage less than 100% indicates the entire surface was not peened one or more times. Surfaces are often peened to achieve coverage greater than 100%; however, overpeening a surface beyond what is necessary for an application can result in crack formation from excessive cold working.

Size and hardness of the shot refers to the characteristic length (typically average diameter for spherical shot) of the peening media and the resistance to localized plastic deformation, respectively. The shot size ranges from 100's of microns to 2 mm. The hardness of the shot depends on the material and is either metal or ceramic. The most common materials are steel and glass.

The nozzle diameter refers to the size of the nozzle where peening media is accelerated and ejected out of nozzle towards a target. Nozzle diameter is typically one-third of the inner diameter of the blast hose in order to achieve maximum shot acceleration [55]. There are two types of pressure blast nozzles: straight bore and venturi bore. Venturi is ideal for delivering a large, uniform blast pattern. A straight bore delivers a more contracted blast pattern meaning that a hot spot forms at the center of the blast area and tapers off at the edges in a Gaussian-like distribution. There preferred nozzle is application dependent. Over time, nozzles wear depending on the shot material and the material of the nozzle. Typically, nozzles are replaced after approximately $1/16^{th}$ of an inch has eroded away. This normally occurs after 500 to 2000 hours of use depending on nozzle material. The nozzles are usually made of wear resistant ceramics, such as tungsten, silicon carbide, or boron.

The air pressure refers to the compressed air supply that acts as a medium to carry the shot and typically ranges from 20 to 100 psi. The air supply must be dry when using air peening. At 100 psi, the shot velocity can reach speeds upwards of 400 mph [56]. It is also important to have a lean shot to air mixture passing through the nozzle. According to I'Anson, "if the shot flow rate is high and the mixture is rich, there will be more solids than

compressible air in the blast hose and therefore the nozzle will not be able to converge and compress the air resulting in a low media exit velocity and possibly unstable media flow."

Impact angle refers to angle formed between the workpiece and the path of the shot projectile [56]. It does not solely refer to the angle of the peening gun with the workpiece since various nozzles, even when perpendicular to the target, have various angles of impingement. Higher angles of impact (flow is perpendicular to the target) will achieve the greatest intensity; however, angles of 80° to 85° are common so that rebounding media do not interfere or collide with incoming media.

The distance between the nozzle and workpiece influences the effectiveness of the peening process. If too close, concentrated severe plastic deformation may damage the surface or the efficiency at peening large areas is too low. If too far, the impact energy is insufficient, which increases the peening time needed.

3.3 Experimental Procedure

3.3.1 Sample Geometry and Preparation

As-rolled sheets of WE43 magnesium alloy (4% Y, 2.5% Nd, 0.5% Zr, 1.2% Gd) used in the present work were bought from China Hunan High Broad New Material Co. Ltd. Samples of dimensions 80 mm × 10 mm × 1mm were cut (Figure 3.3) and polished with a silicon carbide paper of 800 grit size.

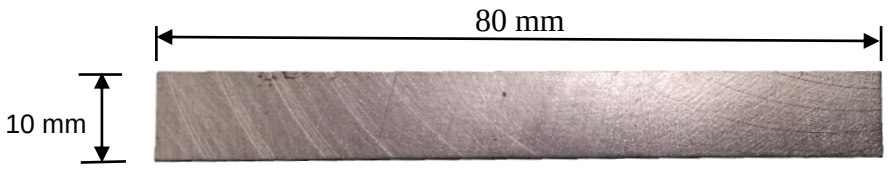

Fig. 3.3 Corrosion and stress-corrosion sample geometry.

3.3.2 Shot Peening Procedure

Magnesium samples were shot peened using a shot peening cabinet with a connected compressor air-line. Glass beads were used to create indentations on the surface instead of stainless steel beads, as the strength and hardness of magnesium is lower than that of steel. Plus, contamination from the steel beads could have affect corrosion behavior by introducing a galvanic cell. The samples were pasted on a block of wood with a double-sided tape during peening. A distance of 15 to 20 cm was maintained between the peening gun and the sample. A pressure regulator was used to adjust the peening pressure. The samples were peened with a static pressure of 20, 40, 60 and 80 psi for 20 seconds on each side.

3.4 Surface Integrity

Surface integrity is the surface condition of a workpiece after being modified by a manufacturing process. This term was coined by Michael Field and John Kahles in 1964. Different aspects of surface integrity include: topography characteristics (surface roughness) and surface layer characteristics (hardness, residual stress). The ability of an implant to integrate into the surrounding tissue depends on its surface integrity [57]. Although SP is a well-established method of surface treating metals, the influence of surface integrity produced by SP on the corrosion rate of that metal is less explored. Hence, this study investigates the surface integrity of magnesium with different peening parameters to further relate it with corrosion rates of the same. Characterization of surface topography, micro-hardness, residual stress, and microstructure has been done in the following sections.

3.4.1 Topography

Surface topography is an important parameter while considering cell attachment on implant material. Shot peening is an efficient way to maintain cell functions and reduce harmful bacteria adhesion [58]. By varying shot peening pressures, surface parameters such as roughness can be controlled. Figure 3.4 shows the surfaces of shot peened samples.

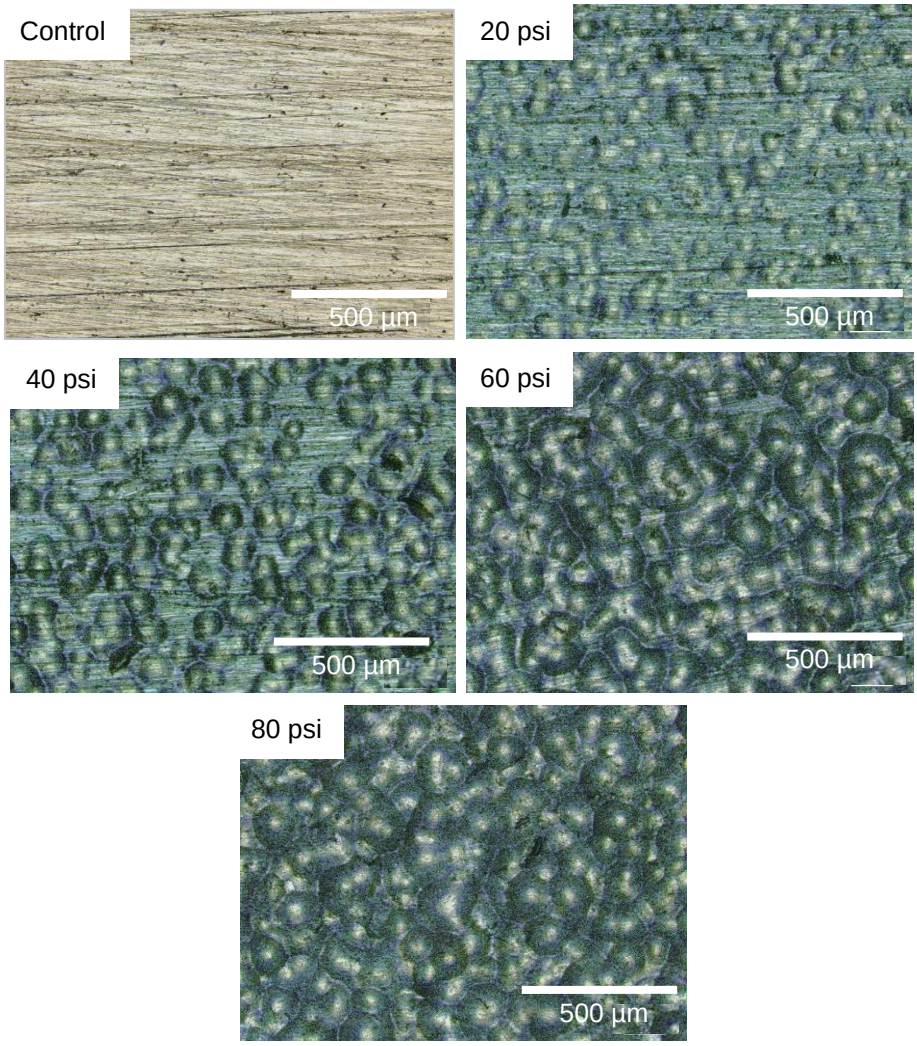

Fig. 3.4 Surfaces produced after shot peening WE43 with different peening pressures.

(a) Measurement Procedure

Keyence laser scanning microscope VK-X200K was used to measure the 3D surface topography of shot peened samples (Figure 3.5). This laser scanning confocal microscope performs non-contact surface profile and roughness measurements. A surface of approximately 1.5 × 1.5 mm^2 was scanned with a magnification of 5X. The arithmetic mean surface roughness (R_a), peak roughness (R_p), and valley roughness (R_v) were analyzed after scanning.

(b) Surface Roughness

VK-Analyzer software was used to find the roughness values. Figure 3.7(a) indicates the arithmetic mean values (R_a) of samples shot peened with different peening intensities. Figure 3.7(b) indicates the peak and valley roughness values of samples. It was observed that R_a increased with an increase in peening pressure. Also, R_p and R_v showed an increasing trend in the values with an increase in peening pressure. However, not much difference was observed in the peak and valley roughness of non-shot peened and shot peened samples.

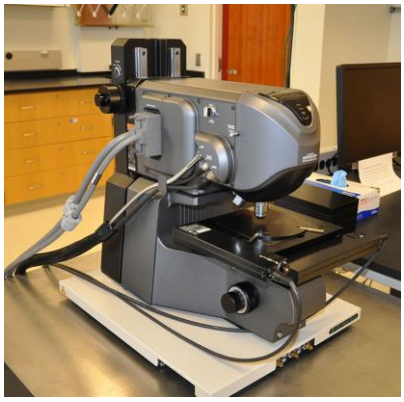

Fig 3.5 Keyence Laser Scanning Microscope VK-200K.

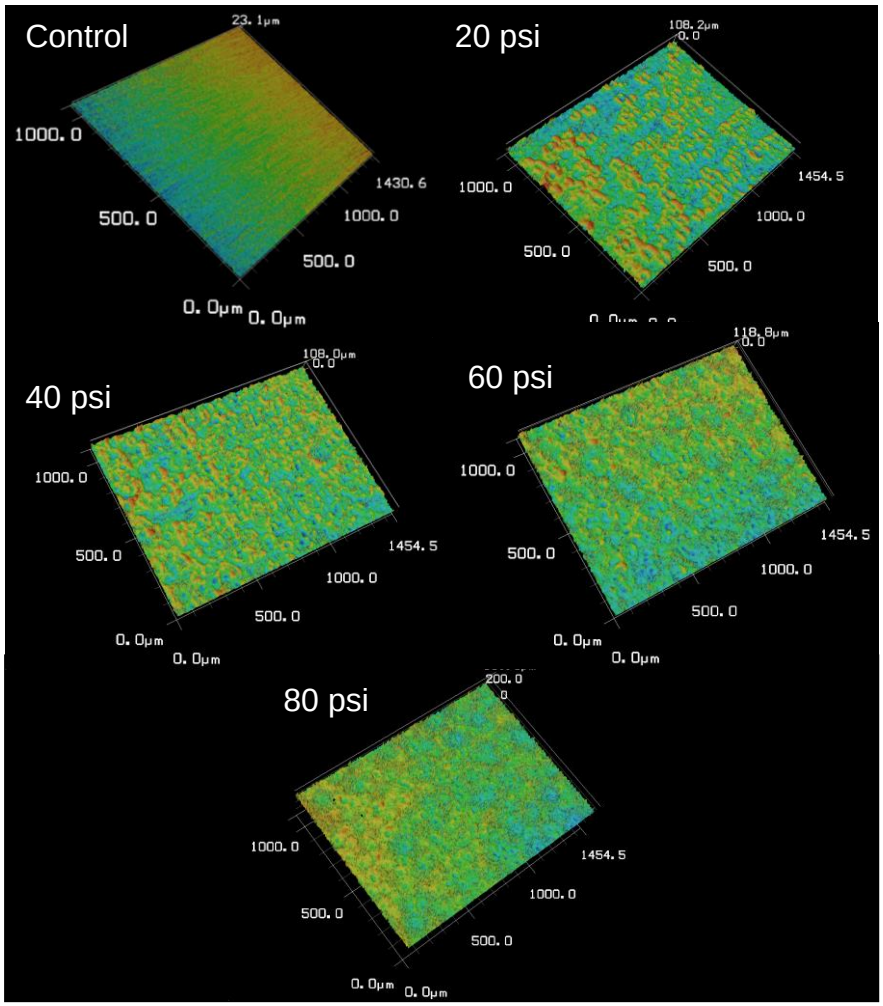

Fig. 3.6 3D topography profiles of shot peened samples.

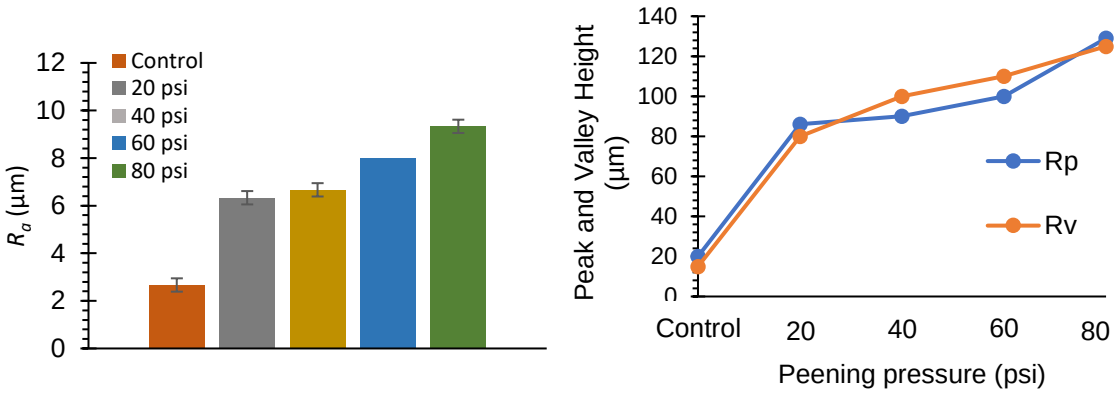

Fig. 3.7 (a) Arithmetic mean roughness values (R_a) and (b) Peak (R_p) and valley roughness (R_v).

(c) Coverage

Coverage is defined as the percentage of area that has been impacted in a given time [59]. Coverage can be controlled by adjusting the time and pressure of peening. As seen in Figure 3.4, although the coverage of samples with 20 psi and 40 psi pressure is not 100%, the surface area of the specimen exposed to the solution varies. In this study, the peening time is kept constant to maintain the same coverage and surface area of the samples. Another alternative is to keep the coverage of all samples the same (100%) and vary the peening time. Both alternatives provide sufficient repeatability to the experiments.

(d) Change in Surface Area

The surface area of the sample increased due to the deformation from shot peening (Table 3.1). The total surface area exposed to corrosion affects the current density (*i.e.* corrosion rate) of the specimen. Hence, it is essential to record this change in surface area to further account it in corrosion rate calculations.

Table 3.1 Change in surface area due to shot peening

Sample	Control	20 psi	40 psi	60 psi	80 psi
Surface Area Ratio	1	1.71	1.94	3.38	4.38
Total surface area (cm^2) exposed to corrosion	5.94	10.15	11.52	20.07	26.01

3.4.2 Microhardness

(a) Measurement Procedure

The Vickers hardness test was used to measure the surface hardness of shot peened magnesium WE43 with different peening intensities. A diamond in the form of a

pyramid base with an angle of 136° between opposite faces was used as an indenter. A test force (F) of 1 gf to 100 kgf was applied according to the material used. The force applied on the indenter created a square mark on the material. The diagonals of this square (d_1, d_2) were measured using a microscope, and the Vickers hardness was calculated using the following formula:

$$HV = \frac{2F \sin\frac{136°}{2}}{d^2} = 1.854\frac{F}{d^2} \tag{3.1}$$

where F = load in kgf

d = arithmetic mean of the two diagonals, d_1 and d_2 in mm

HV = Vickers hardness

In this test, a load of 300 gmf with a load time of 5 seconds was used. An objective of 50X zoom was used to measure the diagonals in order to improve accuracy. Hence, the average diagonal was divided by a factor of 50 in the calculations.

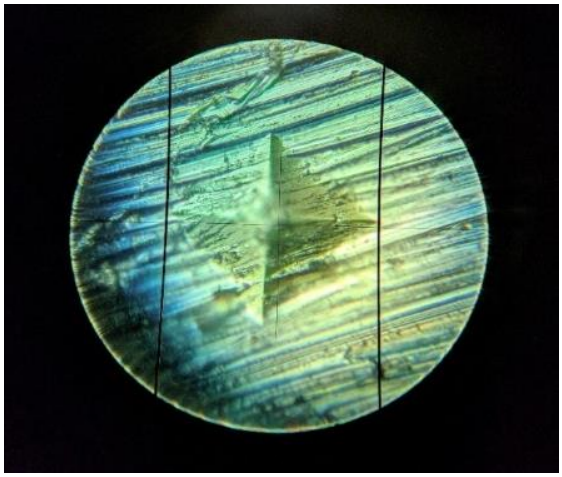

Fig. 3.8 Vickers hardness measurement.

(b) Vickers Hardness Results

The surface hardness for samples shot peened for various peening pressures is indicated in Figure 3.9. It was observed that the Vickers hardness number (VHN) value increased with an increase in peening pressure. Thus, peening the surface of the alloy with a higher pressure of shots increased the hardness of the surface. This suggests that peening a surface with higher pressure could improve the corrosion resistance of an implant.

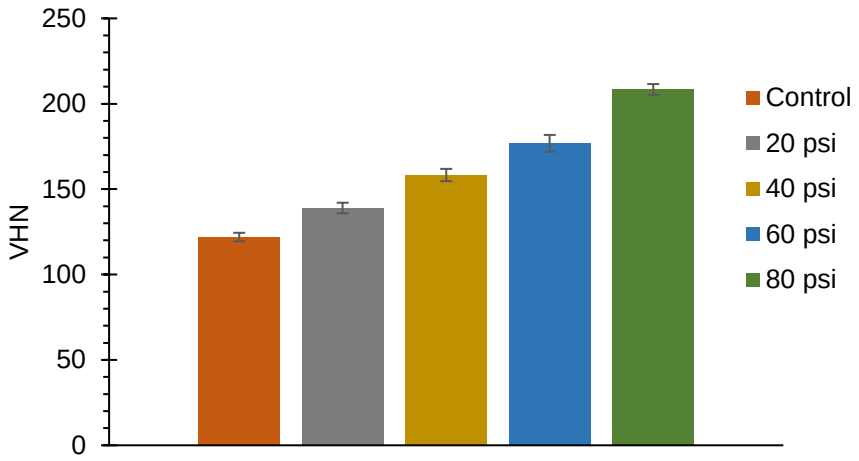

Fig. 3.9 Vickers microhardness on the surface of shot peened WE43 alloy.

3.4.3 Residual Stress Characterization

(a) Purpose of Measuring Residual Stress

Shot peening is one of the common processes to impart residual stress in an object that is subjected to stress corrosion cracking. Although the shot peening process can be governed by monitoring peening intensity, there is no simple relation between the peening intensity and the depth of residual stress induced in the part. The form of the

residual stress-depth curve influences the sample arc height, and equal arc heights can be obtained by various stress distributions. Similarly, shot peening with the same peening intensity but different shot sizes will result in different subsurface residual stresses. The stress distribution by this process depends on the properties of the material used, prior processing, and peening parameters. The shot peening process can be efficiently controlled and optimized by measuring the induced subsurface residual stresses [60].

(b) Measuring Residual Stresses using XRD

Mechanical (dissection techniques) and nonlinear elastic methods (ultrasonic and magnetic techniques) are used to determine the amount of residual stress. Both these methods have limitations, and thus concern the accuracy of residual stress determination. As mechanical methods are necessarily destructive, they cannot check repeatability. Major errors can occur in nonlinear elastic methods due to orientation, grain size, and temperature of the material. Moreover, spatial and depth resolution of these methods are orders of magnitude lower than that of XRD. Thus, x-ray diffraction is a reliable method to quantify subsurface residual stresses induced by surface treatments such as shot peening, laser shock peening, and burnishing [61].

(c) Principle of Measuring Residual Stress

Metals are composed of several crystals oriented in different directions. If an external force is applied, deformation is observed in the lattice spacing (d) of each of these crystals. After shot peening the sample, the layers beneath the surface are compressed, and thus compressive residual stress is induced in the samples. X-rays

penetrate into the sample up to a depth of 10 microns to effectively measure the stress distribution near the surface.

(d) Experimental Setup and Procedure

The residual stress characterization was done on a Rigaku SmartLab Diffractometer in the Nebraska Center for Materials and Nanoscience (Figure 3.10(a)). A Cu Kα source with the wavelength of 1.54 Å was used to scan the sample in the y-direction (Figure 3.10(c)). A Soller slit of 5 mm width was used to scan a 5-mm wide area. Residual stresses were measured at an angle greater than 100° for reliable results. A general measurement indicated that the highest peak was observed at 104° (Figure 3.11).

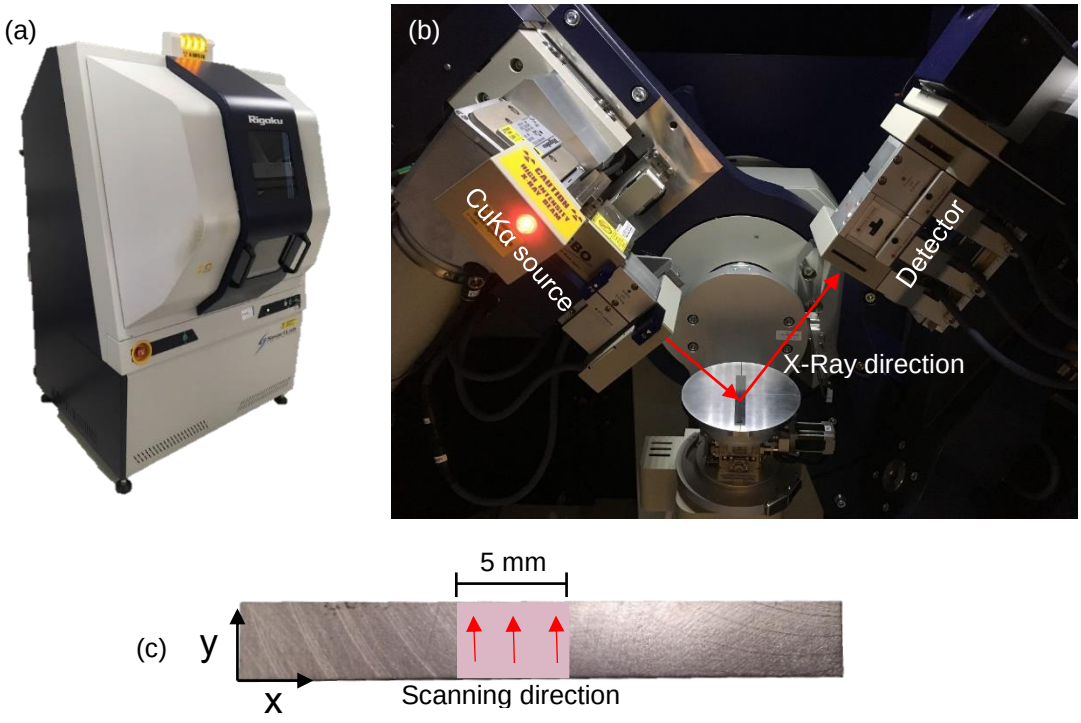

Fig. 3.10 (a) Rigaku SmartLab Diffractometer, (b) experimental diagram of X-Ray scanning, and (c) sample orientation.

(e) Analysis of Data

The samples with different shot peening pressures were scanned at different ψ angles (angle between sample surface normal and lattice plane angle) ranging from -30° to +30°. A graph of 2θ versus $\sin^2(\psi)$ was plotted (Figure 3.12) and the slopes of the lines were used to calculate the residual stress using the following formula from [61, 62]:

$$\sigma = -\frac{E}{2(1+\nu)}.\cot\frac{2\theta_o}{2}.\frac{\pi}{180}.\frac{\Delta(2\theta)}{\Delta\sin^2\psi} \tag{3.2}$$

where $2\theta_o$ = diffraction peak angle when sample is stress-free,

E = Young's modulus (MPa) = 44200 MPa,

ν = Poisson's ratio = 0.27, and

$\frac{\Delta(2\theta)}{\Delta\sin^2\psi}$ = slope of lines in 2θ - $\sin^2(\psi)$ plot.

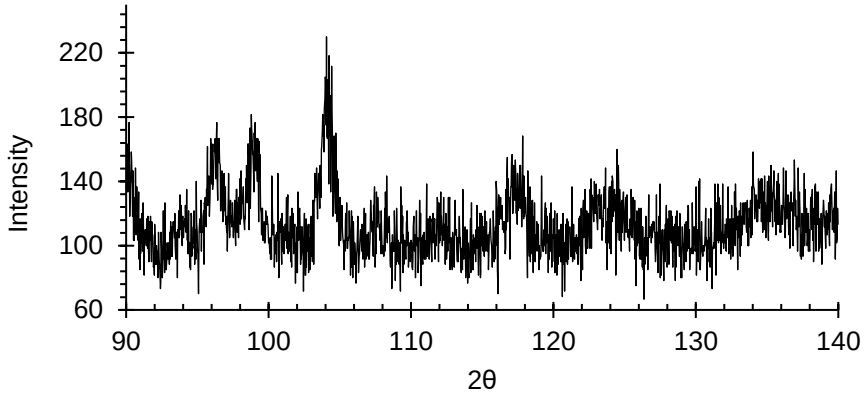

Fig. 3.11 General intensity versus 2θ scan to determine highest peak.

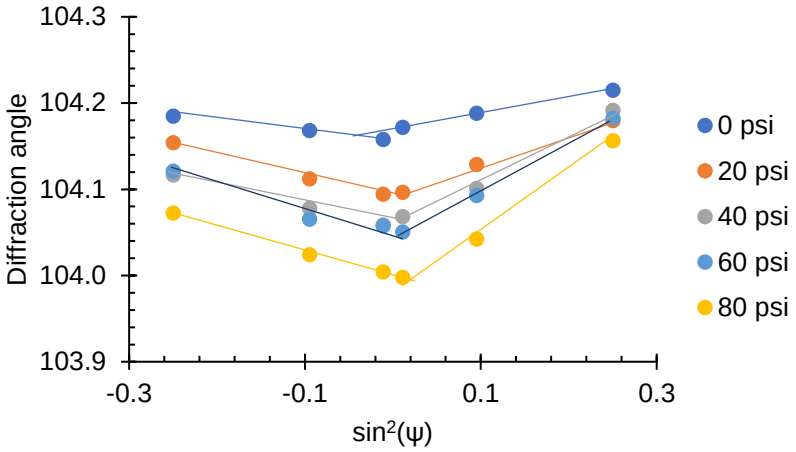

Fig. 3.12 2θ vs. $\sin^2(\psi)$ plot stress analysis.

(f) Results and Conclusions

As observed in Figure 3.12, the slope of lines in the 2θ - $\sin^2(\psi)$ graph increased with an increase in peening pressure. The residual stress values were calculated using Equation 3.2 and the values of residual stresses for different peening pressures were plotted (Figure 3.13).

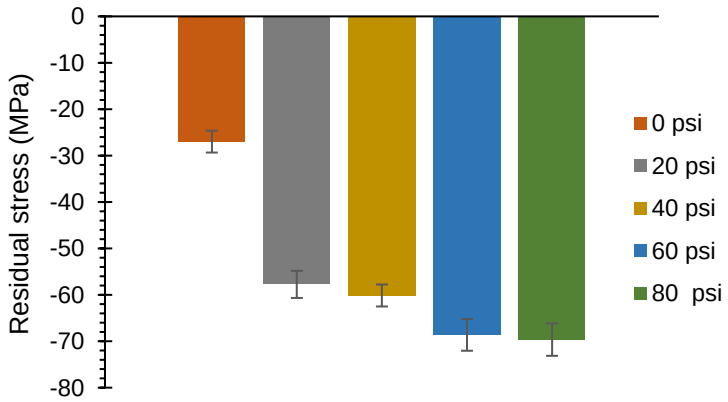

Fig. 3.13 Residual stresses in shot peened magnesium WE43 alloy at peening pressures from 20 psi to 80 psi.

The calculated residual stresses increased with increasing peening pressures. However, the difference between the residual stress values of (a) 20 and 40 psi and (b) 60 and 80 psi was minimal. That could indicate that the samples could be saturated with that peening pressure and time. Moreover, a compressive residual stress of about 20 MPa was observed in a non-shot peened sample. This stress is a result of polishing, cutting, and rolling the samples.

3.4.4 Microstructure

Metallographic etching was used to capture structural characteristics of a metal that were not evident in the as-polished conditions. The experimental setup to etch is shown is Figure 3.14. A solution of 10 ml hydrofluoric acid and 90 ml water was used for etching WE43 (ASTM E407-07). As HF etched through the glass, plastic equipment was used to carry it. This experiment was performed in a fume hood with a ventilation rate of 80 cfm. A polished sample was immersed and gently agitated in this solution for 25 to 30 seconds. The etched surface was then observed under an optical microscope. The grain size ranged from 50 to 150 µm (Figure. 3.15).

Fig. 3.14 (a) Equipment for metallographic etching and (b) fume-hood to perform HF etching.

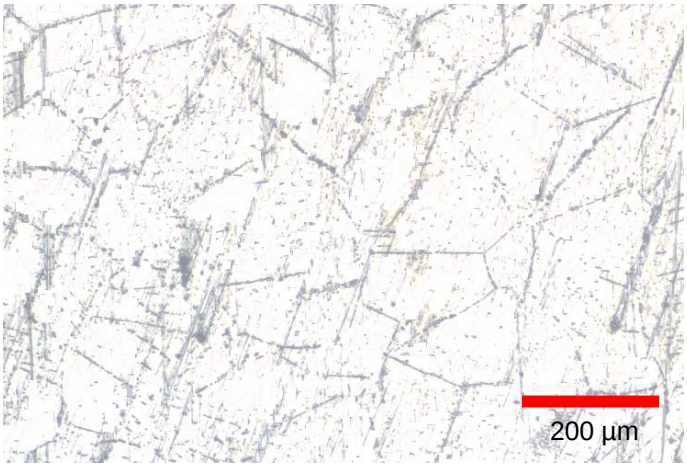

Fig. 3.15 Microstructure of WE43.

3.5 Summary & Conclusions

Shot peening was initiated to modify the surface integrity of magnesium WE43 alloy. Surface topography, hardness, and residual stresses were analyzed using a laser scanning microscope, Vickers hardness tester, and a Rigaku x-ray diffractometer, respectively. It was observed that roughness and microhardness increased with increase in shot peening pressure on the magnesium samples. An increasing trend in the residual stress was also observed. It indicates that the residual stresses in the magnesium samples became more compressive with increasing peening pressure.

CHAPTER 4

CORROSION RESISTANCE OF SHOT PEENED MAGNESIUM WE43

4.1 Introduction

It is essential to determine the corrosion rate of a magnesium alloy to relate its corrosion behavior to its composition, microstructure, and surface chemistry. In the case of orthopedic implants, corrosion behavior depends on the surface treatment or coating on the implant. Hence, measuring corrosion rate while analyzing the surface integrity of an alloy is required to find a relationship between these two important parameters.

The corrosion rates of magnesium alloys are higher than other engineering alloys, as the cathodic reaction is a water reduction (producing H_2). Hence, uniquely for magnesium alloys, different techniques have been designed for corrosion assessment. This chapter discusses some of the techniques used for finding corrosion rate of magnesium. The corrosion rate results using one of these techniques, *i.e.*, potentiodynamic polarization, are discussed in this Chapter.

4.2 Literature Review: Measurement of Corrosion Rate

In vivo corrosion measurement is required for successfully designing orthopedic implants. Investigation of *in vivo* corrosion rate of different magnesium alloys has been done by Witte and Kaese [63]. However, the first step in the development of implants is to find the *in vitro* corrosion rate of an alloy. The difference between measurement of corrosion rates of magnesium alloys *in vivo* and *in vitro* conditions has been explained by Witte *et al.* [64].

Different methods of corrosion rate assessment have been discussed in some recent

reviews. Kirkland *et al.* reviewed the methodologies used to study the corrosion of magnesium implant materials [65]. The fundamentals of some scanning probe techniques in magnesium corrosion research were discussed by Dauphin in [66]. Various experimental and analytical tools for corrosion testing of magnesium alloys have been discussed in [67]. A list of various corrosion measurement techniques is shown in Figure 4.1.

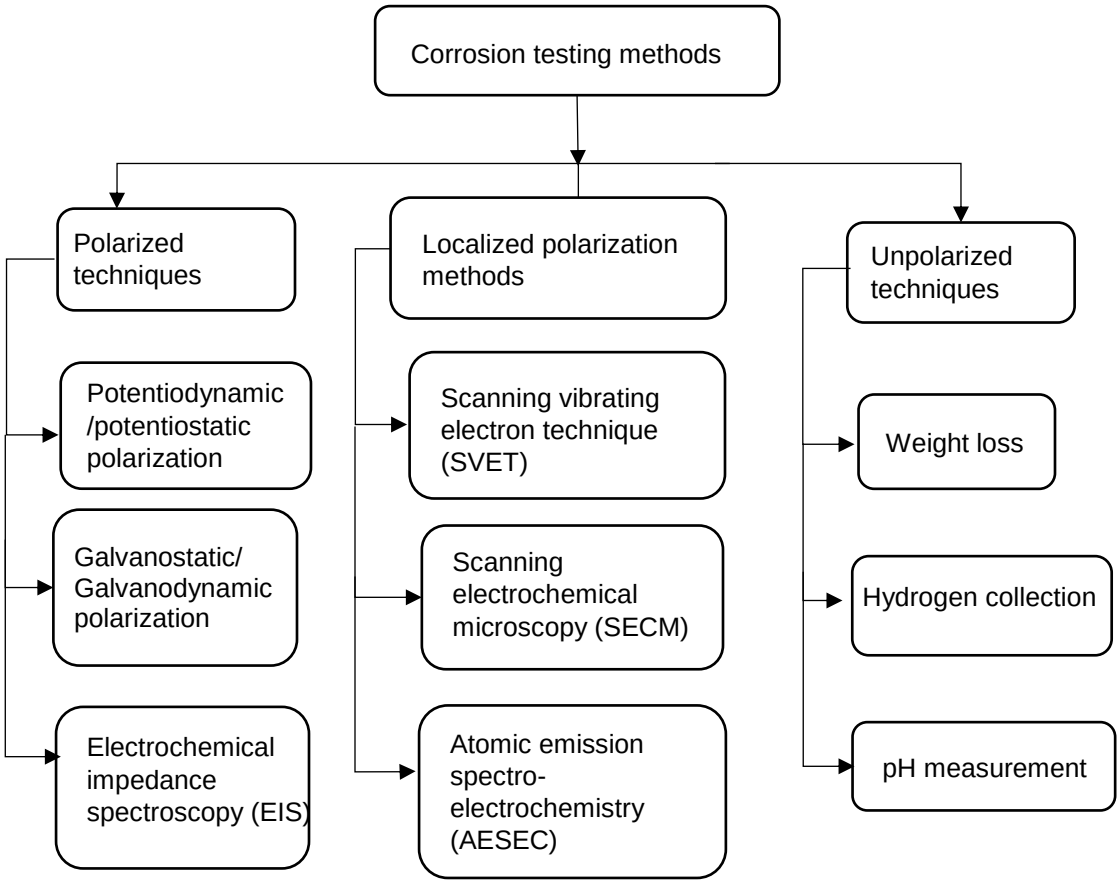

Fig. 4.1 List of corrosion measurement techniques. Modified from [65-67].

4.2.1 Polarization Techniques

Polarized experiments require special equipment such as potentiostat or galvanostat. They give information on the instantaneous corrosion rate of the alloy. The

experimental setup is relatively easy, and these techniques are used to determine the anodic and cathodic rate of corrosion reactions [67]. As polarization experiments are accelerated by applying voltage or current, they do not simulate the exact physiological conditions in a human body. However, they provide a good overall picture while comparing corrosion rates of samples peened with different intensities.

(a) Potentiodyamic Polarization (PDP)

External voltage difference is applied in between the reference electrode, working electrode, and the counter electrode over a fixed rate. This method has gained popularity due to its ability of calculating anodic and cathodic kinetics easily. Tafel extrapolation or linear polarization resistance method (LPR) can be used to find the instantaneous corrosion rate of the material. This method can compare the effect of changes in the system, such as change in pH of solution or change in surface integrity of a specimen.

Figure 4.2 shows the effect of change in concentration of the electrolyte (NaCl) on the degradation of pure magnesium [68]. Here, different concentration levels correspond to different pH levels of the solution. It was observed that the current density of magnesium (i_{corr}), which is directly proportional to the corrosion rate of magnesium increases as the concentration of solution increases. At the same time, more negative voltage is required to corrode the metal (V decreases). Hence, the corrosion resistance of magnesium decreases. This result aligns with the fact that the metal becomes more susceptible to corrosion when more salts are added to the solution. Thus, PDP is an easy way to compare different changes in the system.

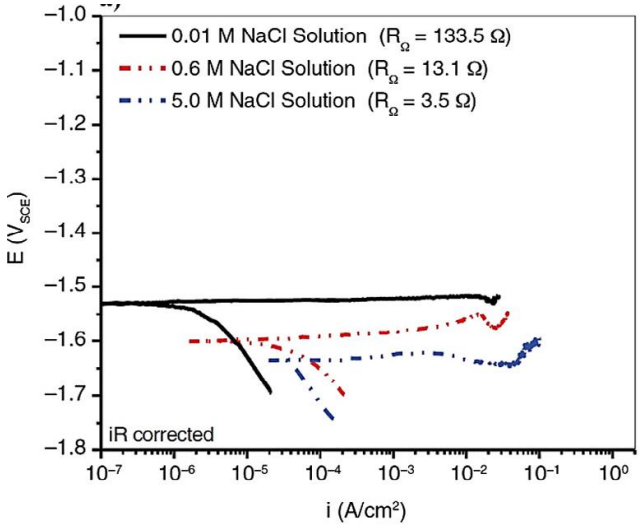

Fig. 4.2 Polarization curves showing the effect of NaCl concentration on corrosion rate of commercially pure magnesium [68].

(b) Potentiostatic Polarization (PSP)

This method uses the same basic principle as that of PDP, but the potential applied is fixed and the current is measured. PSP can be used to study hydrogen evolution during anodic polarization [69] or to measure the voltage and current while coating magnesium surfaces [70].

(c) Galvanodynamic Polarization

As current and voltage are mutually independent in electrochemical reactions, controlling one of them and measuring another is easy. In most methods, voltage is controlled and current is measured with the advent of potentiostats. The reason behind this is that, in certain conditions multiple potentials correspond to the same current. The current control method can sometimes provide a multi-valued function of current. Also, current control method does not detect passivation.

Constant or variable current is applied in galvanostatic and galvanodynamic methods, respectively. These methods are widely used in magnesium corrosion as they are less complicated and since magnesium passivates at a very high pH.

(d) Electrochemical Impedance Spectroscopy (EIS)

EIS is one of the theoretically complex and expensive methods used for corrosion rate analysis. This method consists of measuring the response of an electrode to a small amplitude (5 to 25 mV) sinusoidal potential perturbation at different frequencies. It can distinguish between two or more electrochemical reactions taking place in the system simultaneously. EIS can provide data on capacitive behavior of the system and can identify diffusion-limited reactions. The kinetics of corrosion are plotted using Bode plot or Nyquist plot. Figure 4.3 shows a Nyquist plot pure magnesium after 24 hours of immersion in a 0.1 M NaCl solution at low frequency.

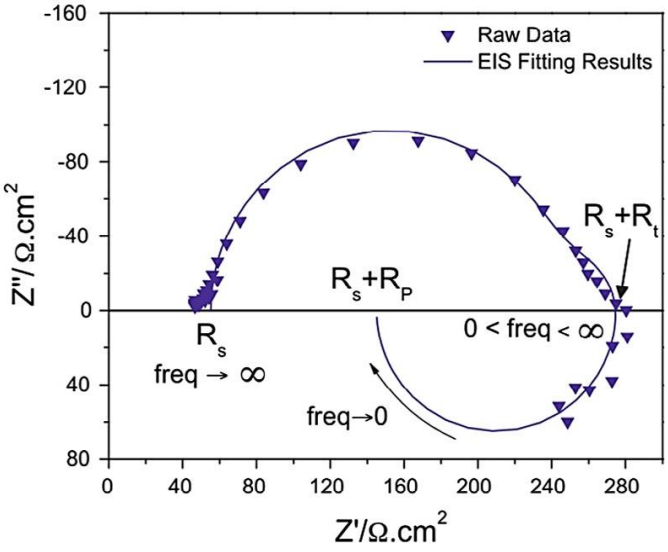

Fig 4.3 Nyquist plot of pure magnesium.

4.2.2 Localized Electrochemical Techniques

Localized electrochemical methods are used to find the corrosion rate in cases of localized corrosion. Different techniques include the following: scanning vibrating electrode technique (SVET), scanning electrochemical microscopy (SECM), and atomic emission spectro-electrochemistry (AESEC). SVET uses a vibrating microprobe to detect the local electrochemical activity on a metal surface by measuring the local voltage drop in a solution. SECM uses an ultra-microelectrode (UME) to scan the metal surface from a fixed height. The electrochemical response of the probe in the proximity of the metal surface is measured. AESEC is one of the most accurate methods for measuring localized corrosion. This method allows the real-time measurement of the partial elemental dissolution rates in the absence of polarization [66].

4.2.3 Non-Electrochemical Techniques

Non-electrochemical immersion tests are commonly used for corrosion rate measurement of magnesium by weight loss method, hydrogen collection method, and by pH measurements. These methods simulate the actual physiological conditions; however, they take a longer time for corrosion. Many times, multiple types of immersion tests are combined to find an accurate corrosion rate; *e.g.*, weight loss and hydrogen collection.

(a) Mass Loss Method

In this technique, the specimen weight and geometry is recorded before and after corrosion. Corrosion can be observed by immersing the sample into simulated physiological conditions; *e.g.*, Hanks' balanced salt solution. After exposing the sample to

the corrosive environment, it is necessary to clean the sample to remove corrosive products from the surface for measuring the weight after exposure. This is an important step to accurately measure the amount of degradation. For magnesium, dilute chromic acid can be used to clean the surface of a sample. Although mass loss method cannot give any data on corrosion kinetics and provides an average corrosion rate, it is considered as a more accurate method for corrosion rate evaluation.

(b) Hydrogen Collection

The cathodic reaction of magnesium is a water reduction reaction that contains dissolution of Mg and results in the evolution of hydrogen (Chapter 1, Section 1.1.4). Thus, the volume of hydrogen collected corresponds to the corrosion rate of magnesium.

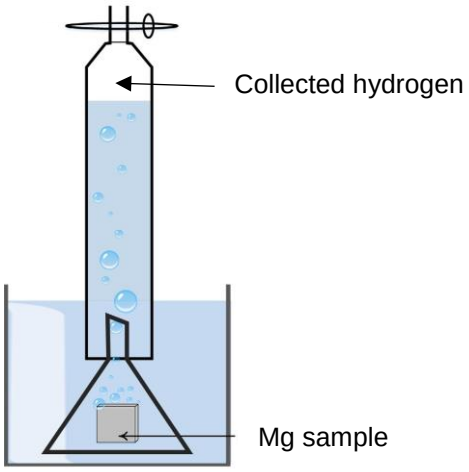

Fig. 4.4 Volumetric method of hydrogen collection.

Hydrogen collection can be done by volumetric method or gravimetric method. The volumetric method is simple and commonly used for magnesium. The corroding sample is covered by a funnel inserted in an inverted burette (Figure 4.4). The hydrogen

gas resulting from the corrosion reaction accumulated on the sample in the form of bubbles, which get accumulated and eventually detached from the surface. These bubbles are then collected inside the inverted burette. Gravimetric method is a real-time hydrogen collection method that measures buoyancy force resulting from the accumulation of hydrogen in a submerged container. The corrosion rate of magnesium is calculated from the volume of hydrogen gas collected for a given amount of time.

(c) pH Measurements

This technique assesses the corrosion rate of dissolving magnesium by chemical titration. As corrosion reaction proceeds, the pH of the electrolyte increases. The pH of electrolyte is kept constant by adding an appropriate solution as a titrant. The volume of titrant added corresponds to the amount of charge consumed in the reaction [71]. The metal hydrolysis influences pH of the solution, thus introducing measurement error.

4.3 Corrosion Tests

Potentiodynamic polarization technique (PDP) was used to compare the effect of shot peening on the corrosion rates of magnesium WE43. A conventional three-electrode cell was used on a Gamry 1100E Potentiostat to conduct corrosion tests. The counter electrode was made of graphite and the reference electrode was saturated calomel electrode. The electrolyte used was as a 0.5% NaCl at a temperature of 37°C. Shot peened samples with peening pressure of 20, 40, 60, 80 psi were polarized. The PDP scans were performed with the scan rate of 1 mV/s with the potential range from -3 to 1 V. Figure 4.5 indicates the schematic and experimental setup of the polarization test. The pH of solution

was checked after every test and was maintained in the range of 7 to 7.8. The solution was discarded if pH rose beyond the limit. Each polarization test was repeated three times.

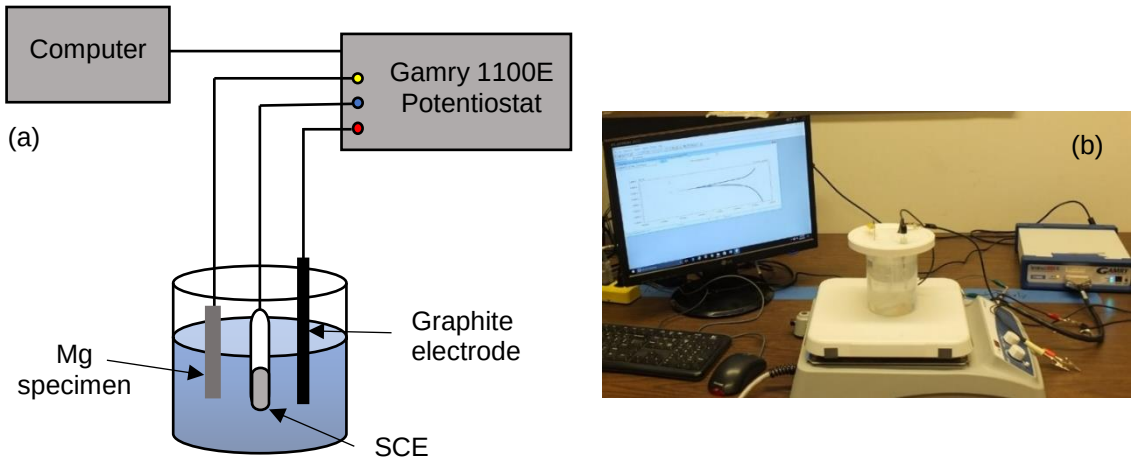

Fig. 4.5 (a) Three-electrode potentiodynamic polarization test; (b) experimental setup of polarization test in the lab.

4.4 Results: Effect of Shot Peening on Corrosion Rate of Magnesium WE43

Shot peening (SP) increased the surface area of the samples with increase in peening pressure. Hence, the surface area exposed to sample peened with different intensities was different (Table 4.1). Thus, the surface area of a shot peened sample with 80 psi intensity increased approximately 4.38 times.

Table 4.1: Surface area ratios of samples with different peening pressures

Sample	Control	20 psi	40 psi	60 psi	80 psi
Surface area ratio (S)	1.00	1.71	1.94	3.38	4.38
Total surface area exposed to solution (cm^2)	5.94	10.15	11.52	20.07	26.01

The current density was calculated as:

$$i = \frac{I\ (\text{instantaneous current values})}{A\ (\text{surface area exposed to solution})} = \frac{I}{S \times A_0} \qquad (4.1)$$

where i = current density (A/cm^2), I = instantaneous current density (A/cm^2), A = total surface area exposed to the solution, S = surface area ratio, A_0 = projected area of sample.

Figure 4.6 shows the potentiodynamic polarization graph (V *vs* log i) of samples with different peening pressures considering the increase in surface area. Tafel extrapolation was used to find the voltage (E_{corr}) and current density (i_{corr}) for different peening pressures. The results of Tafel extrapolation are indicated in Table 4.2. The current density of samples shot peened with different peening pressure are shown in Figure 4.7.

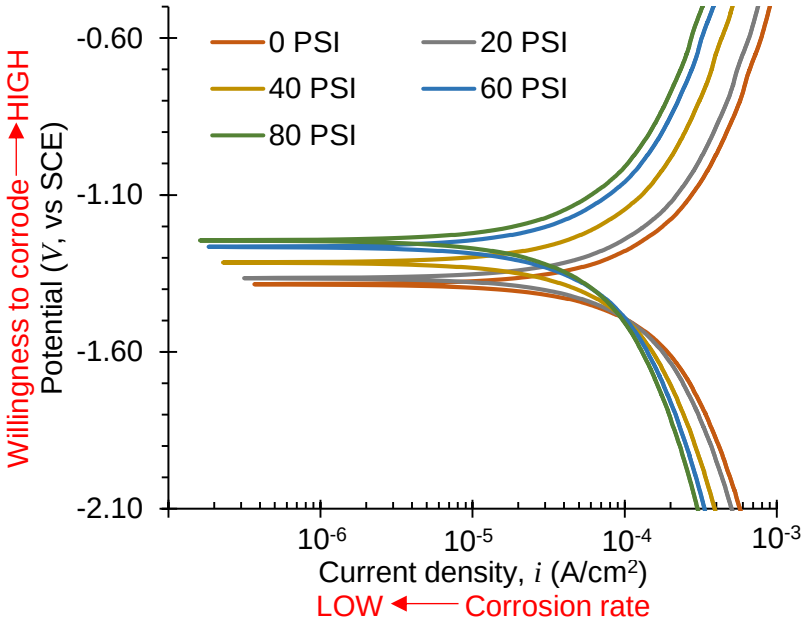

Fig. 4.6 Potentiodynamic polarization of shot peened WE43 with different peening pressure.

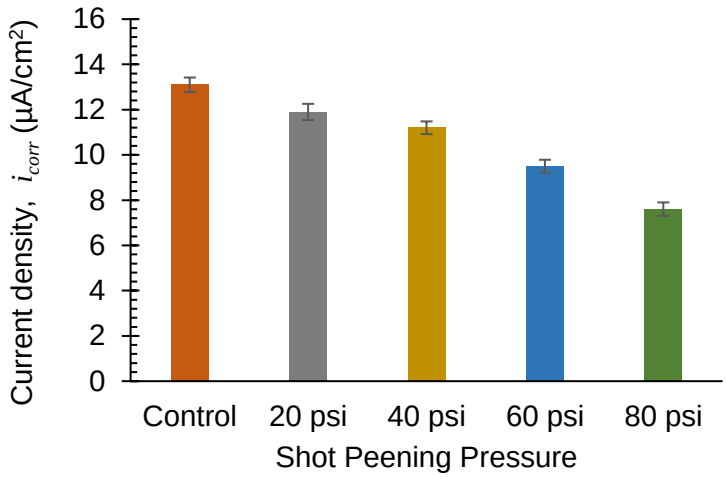

Fig. 4.7 Current densities of samples shot peened with different peening pressure.

Table 4.2: Tafel extrapolation results of samples considering the change in surface area

	Control	20 psi	40 psi	60 psi	80 psi
E_{corr} (V)	-1.41	-1.39	-1.32	-1.24	-1.23
i_{corr} (µA/cm²)	13.1	11.9	11.2	9.5	7.6

It was observed that the corrosion potential increased (more noble) with higher shot peening pressure, *i.e.*, samples became less willing to corrode with higher peening pressure. Moreover, the current density (*i.e.* corrosion rate) decreased with higher peening pressure (Figure 4.7).

4.5 Summary and Conclusion

Magnesium WE43 samples were peened with different peening pressures. The surface integrity as well as the surface area of exposure to the solution were different due indentations. It is essential to consider this change in surface area of samples as it directly affects the corrosion rate. Potentiodynamic polarization tests were performed to observe the effect of shot peening on the corrosion rate of WE43. Tafel extrapolation method was

executed to find the corrosion potential (E_{corr}) and corrosion current density (i_{corr}) of samples. The results indicated that the corrosion potential increased, while the current density decreased with higher peening pressures. The increase in corrosion potential (E_{corr}) implied that the samples became less willing to corrode, while the decrease in current density (i_{corr}) implied that the corrosion rate of samples decreased with higher peening pressure. Thus, the samples became more resistant to corrosion.

CHAPTER 5

STRESS CORROSION CRACKING BEHAVIOR OF SHOT PEENED MAGNESIUM WE43

5.1 Introduction

Magnesium alloys are considered as potential biodegradable materials for temporary implantation. The implant material is required to possess adequate resistance to cracking or fracture in physiological environments. Stress corrosion cracking (SCC) and corrosion fatigue (CF) are the two important mechanisms that lead to failure in implants. It is required to consider the effect of external stress or fatigue on the corrosion behavior of the implant. At the same time, it is also required to understand the effect of residual stresses imparted due to shot peening on the corrosion resistance of the implant. In this chapter, the focus has been made on understanding the effect of external stresses and residual stresses on the corrosion behavior of the alloy using potentiodynamic polarization (PDP).

5.2 Materials and Methods

5.2.1 Application of Physiological Environment

(a) Design of Saline Chamber

A saline chamber was designed for application of corrosive environment to the magnesium alloy samples (Figure 5.1). The chamber was made of a square acrylic tube to carry corrosive fluid. A rectangular slot of 10 mm × 1 mm was designed to hold the sample while applying a uniform load. To make the chamber leakproof, a rubber O-ring of 1 mm

diameter was attached to both ends of the magnesium sample. A set of plates and screws was used to apply compressive force on the O-rings. Due to this compressive force, the O-ring was deformed, thus covering the leak between sample and saline chamber. Care has been taken that the O-ring did not apply an external force on the sample.

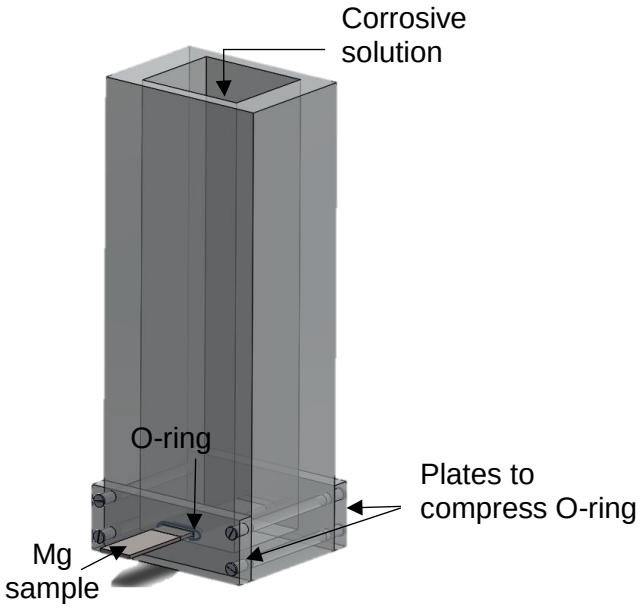

Fig. 5.1 Solid model of saline chamber on SolidWorks.

(b) Simulated Body Fluids

To simulate body fluids in these experiments, Hank's powders and Hank's ready - made solution is generally used. A white residue was observed in the solution after keeping samples of WE43 for a longer duration (5 to 7 hours). To avoid any kind of errors, 0.5 % NaCl was used in these experiments.

(c) Maintain Temperature and pH of the Solution

To simulate body conditions, the temperature of solution was maintained to 37 degrees Celsius. As the pH of the human body remains within a range of 7.35 to 7.45,

pH higher than 8.0 is considered harmful for the body. For these experiments pH was kept in a range of 7.2 to 8.0.

5.2.2 Application of Stress

(a) Maximum Permissible Stress

The yield stress of WE43 is 160 MPa. Thus, the total stress applied to the specimen is required to be lower than the yield stress to be in the elastic region.

The average weight of an American woman over the age 20 and height 5 feet 3 inches is approximately 160 lbs (711.7 N). Considering the entire weight of the body is subjected to the implant during the gait. As the cross-sectional area of the sample was 10 mm^2, the stress induced in implant was 71.17 MPa (~72 MPa). Considering a factor of safety of 0.1, the total stress of 80 MPa was applied. As the stress imparted was lower than the yield stress of the material, all experiments were done based on this stress value. Thus, maximum permissible stress in the specimen was σ_{max} = 80 MPa.

(b) Design of Stress-Frame

A custom-made frame was designed to apply uniaxial stress (Figure 5.2). This type of spring-loaded stress frame has been adapted to stress-corrosion testing as it is simple, compact, and easy-to-use. Force was applied by tightening the nut on one side of the frame and is determined by measuring the deformation of a tension spring on the other side of the frame. The nuts and bolts used were metric, *i.e.,* one rotation of nut corresponded to 1 mm displacement on the bolt.

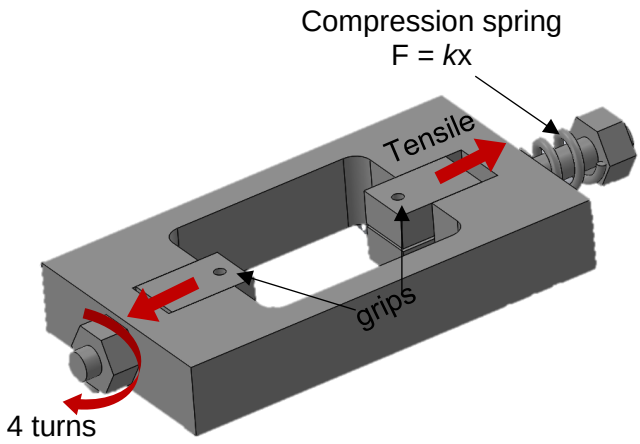

Fig 5.2 Solid model of tensile stress frame on SolidWorks.

In these experiments, a spring made of OTCS (oil tempered chrome silicon) with a spring constant (*k*) of 200 N/mm (free length = 25.4 mm, outer diameter = 18.5 mm, no. of coils = 3) was used. The nut was rotated 4 times to apply a stress of 80 MPa.

5.3 Polarization Tests to Measure Stress-Corrosion Behavior

5.3.1 Experiment Arrangement

To compare the corrosion rates of a surface treated sample with a plain sample, potentiodynamic polarization (PDP) technique was used. A conventional three-electrode cell was used on Gamry 1100E Potentiostat to conduct potentiodynamic polarization tests. The counter electrode was made of graphite and the reference electrode was saturated calomel electrode. The electrolyte used was 0.5% NaCl at a temperature of 37°C. All specimens were cleaned in distilled water and acetone at room temperature before the polarization tests to avoid contamination. The schematic diagram and the experimental setup is shown in Figure 5.3.

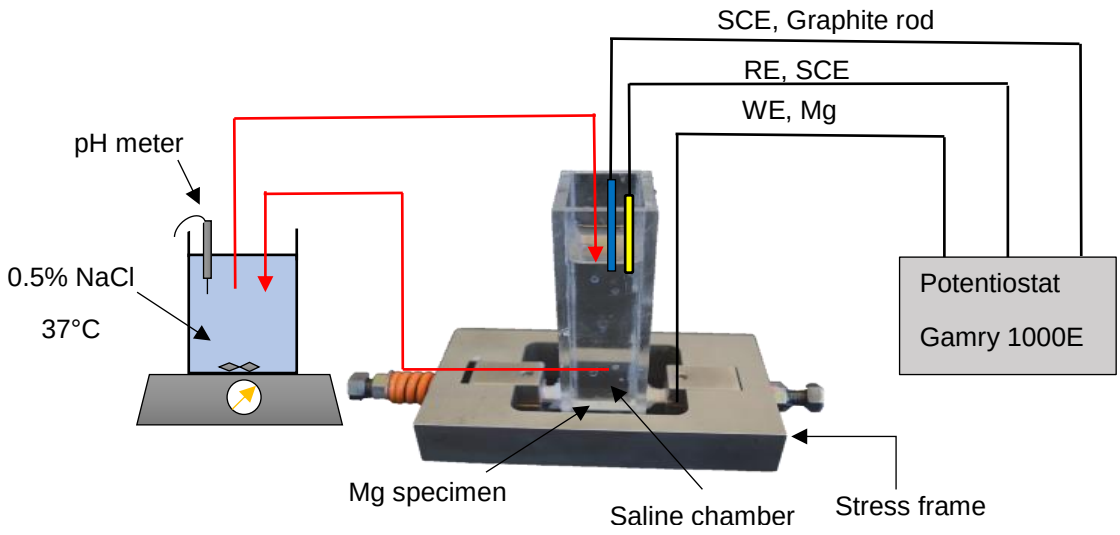

Fig. 5.3 Potentiodynamic polarization arrangement of stressed WE43 samples.

5.3.2 Procedure to find Corrosion Rate:

Shot peened samples with peening pressures of control, 20, 40, 60 and 80 psi were polarized to analyze the effect of external stress and residual stresses on the samples. The surface roughness, surface residual stresses, microstructure, and topography of shot peened samples with different intensities were discussed in Chapter 3. To analyze the effect of peening pressures on the stress corrosion behavior of the alloy, an external stress of 80 MPa was applied to the peened samples along with the corrosive environment. To analyze the effect of external stresses, different external stresses were applied to shot peened samples with 80 psi peening pressure. Tafel extrapolation was used to find the current density and potential of corrosion.

5.3.3 Effect of Peening Pressure on the Stress Corrosion Behavior of WE43

Samples shot peened with peening pressures 0, 20, 40, 60 and 80 psi were inserted in the saline chamber and the stress frame. The surface area of samples exposed

to the solution was different for different peening intensities. The change in surface area for each sample was accounted in the polarization curves. External stress of 80 MPa was applied to the samples to incorporate stress corrosion cracking. Figure 5.4 indicates the potentiodynamic polarization curves for samples shot peened with different peening pressures. Tafel extrapolation was used to calculate corrosion potentials and current densities. Table 5.1 shows the results of Tafel extrapolation results from polarization data. The current density of samples shot peened with different peening pressure is shown in Figure 5.5.

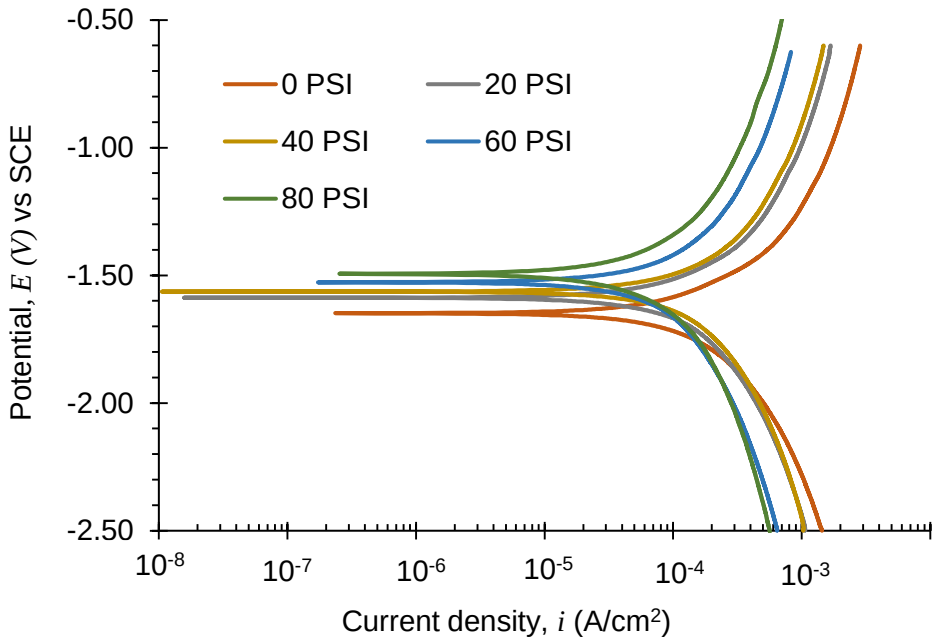

Fig 5.4 Potentiodynamic polarization curves for different shot peening pressures.

Table 5.1 Tafel extrapolation results for different peening pressures

	Control	20 psi	40 psi	60 psi	80 psi
E_{corr} (V)	-1.65	-1.58	-1.56	-1.53	-1.49
i_{corr} (μA/cm^2)	33	24	22	18	11
Area (cm^2)	5.94	10.17	11.52	20.09	26.05

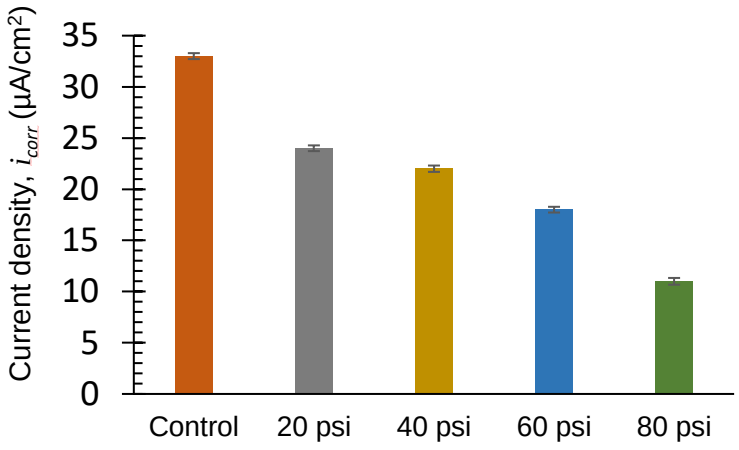

Fig 5.5 Current density, i_{corr} at different shot peening pressures.

It was observed that the corrosion potential (E_{corr}) increased (more noble) with higher shot peening pressure, *i.e.*, samples became less willing to corrode with higher peening pressure. At the same time, the current density (*i.e.* corrosion rate) decreased with higher peening pressure (Figure 5.5).

5.3.4 Effect of External Stress on the Stress-Corrosion Behavior of WE43 at 80 psi Peening Pressure:

Different external stresses (0, 40, 80 MPa) were applied to samples shot peened with 80 psi peening pressure. Since the peening pressure of samples was the same, the surface area exposed to the samples was considered the same. Figure 5.6 shows the polarization curves of samples peened with 80 psi pressure at different external pressures. The Tafel extrapolation results are indicated in Table 5.2

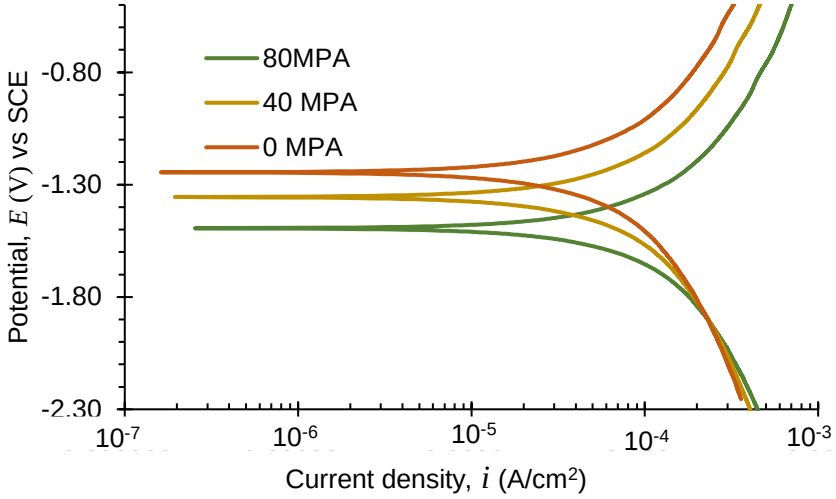

Fig 5.6 Potentiodynamic polarization curves for different external stresses.

Table 5.2 Tafel extrapolation results for different external stresses

	0 MPa	40 MPa	80 MPa
E_{corr} (V)	-1.22	-1.35	-1.49
i_{corr} (μA/mm²)	7.6	9.2	11.3

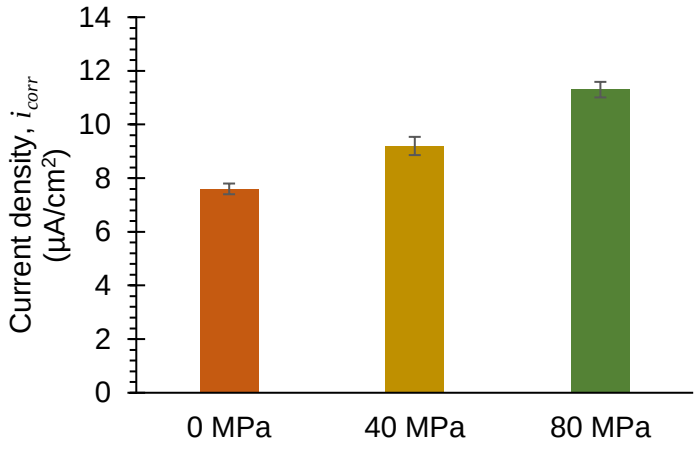

Fig 5.7 Current density, i_{corr} at different external stresses.

The corrosion potential (E_{corr}) of the samples decreased as the external stress applied to sample increased (samples became more active), *i.e.,* samples became more willing to corrode. The current density (i_{corr}) increased with higher external stress (Figure 5.7), *i.e.,* the corrosion rate increased with higher external stress.

5.4 Summary and Conclusions

Shot peening of a biodegradable WE43 alloy has been initiated to modify the surface integrity and to measure the resulting instantaneous stress corrosion behavior. To mimic human physiological loading conditions, a customized stress frame and a corrosion chamber were built. Results indicated that the corrosion resistance of the alloy increased as the pressure of shot peening increased. It was also observed that external stress on the WE43 samples caused a negative shift of corrosion potential and enhanced the corrosion activity as demonstrated through the potentiodynamic polarization results.

5.5 How Experimental Data can be used to Model SCC?

In the assessment of corrosion rate for implants, the effect of elastic stress is required to be considered to calculate the part life. The synergistic effect of corrosion and elastic stress on structures could significantly affect the accuracy during part life assessment. Corrosion models have been designed to extrapolate the corrosion results and find the life of the implant. Various corrosion models such as power function, exponential function, Weibull function can be used to calculate the life of an implant using potentiodynamic polarization results [72].

CHAPTER 6

SUMMARY, CONCLUSIONS, AND RECOMMENDATIONS

6.1 Summary and Conclusions

Shot peening of biodegradable WE43 was initiated to modify the surface integrity and to measure the resulting instantaneous stress-corrosion behavior by potentiodynamic polarization (PDP). A customized stress frame and a corrosion chamber was designed and built to mimic human physiological loading conditions. Results indicated that the corrosion resistance of the alloy increased as the shot peening pressure increased and was inversely proportional to the applied load.

6.1.1 Effect of Stress on Corrosion of Magnesium WE43

To design a medical device for load bearing applications, it is important to consider the effect of external stress on the corrosion rate of the material. While it is predicted that the corrosion rate would increase in presence of stress, there are very few studies that observe the effect of stress on corrosion. Results from this study indicated that the stress-corrosion rate was typically 2 to 3 times higher than the corrosion rate (Figure 6.1).

6.1.2 Linking Shot Peening – Surface Integrity – Stress Corrosion

One of the objectives of this study was to find a relation between *process* (shot peening) – *property* (surface integrity) – *performance* (stress-corrosion rate), *i.e.*, to find the correlation between surface integrity parameters and stress-corrosion rate of magnesium. Surface integrity parameters such as surface roughness (R_a), microhardness

(VHN), and compressive residual stresses were taken into consideration. It was observed that surface roughness, microhardness, and compressive residual stresses increased with higher peening pressure (Figure 6.2), while the stress-corrosion rate decreased with higher peening pressure (Figure 6.1).

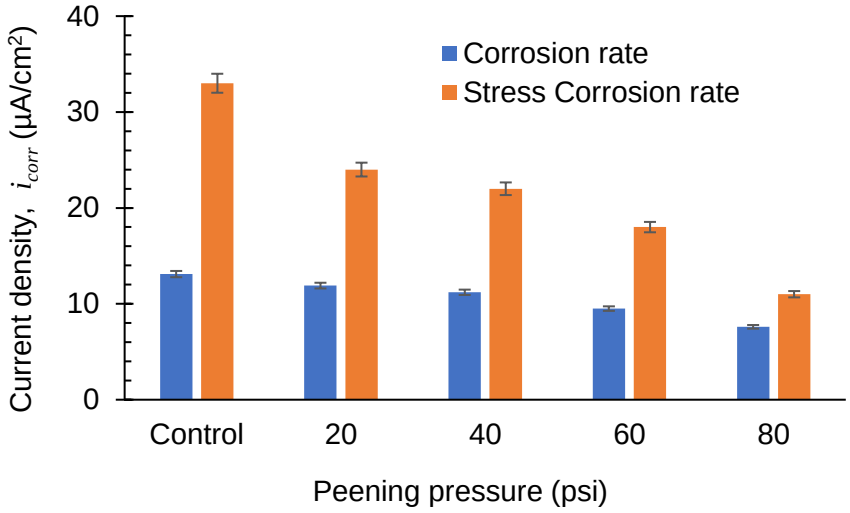

Fig. 6.1 Effect of stress on samples shot peened with different peening pressures.

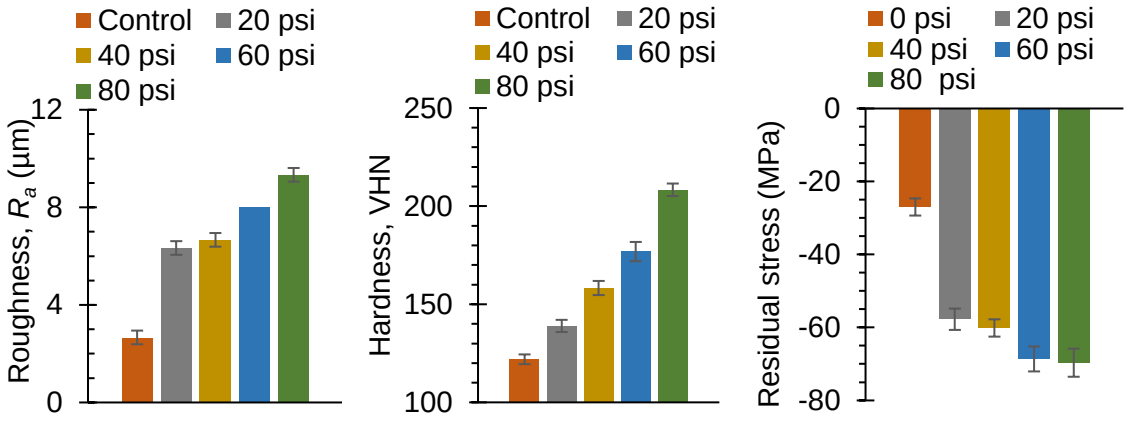

Fig. 6.2 Effect of shot peening pressure on surface integrity parameters.

6.1.3 Understanding Corrosion Rate of Magnesium after Shot Peening

It is necessary to compare corrosion rate of a peened and an unpeened sample to understand the effect of peening on corrosion behavior. According to Faraday's law, the corrosion rate of magnesium is given by:

$$r = \frac{m}{tA} \tag{6.1}$$

where, m: mass lost during corrosion, t: corrosion time, A: actual surface area exposed to the solution (not the projected surface area). The subscript "p" and "up" refers to peened and unpeened, respectively.

If time (t) for which both the samples are corroded is kept constant, the corrosion rate only depends on the mass of material lost and surface area exposed to the sample. The surface area of peened sample was higher than the surface area of the unpeened sample ($A_p > A_{up}$). To understand how mass loss (m) affects the corrosion rate, the following three cases were considered:

1) When $m_p > m_{up}$: Although the peened sample corrodes more and loses more amount of mass, the corrosion rate of a peened sample could still be lower than the unpeened sample if the ratio of $(m/A)_p < (m/A)_{up}$.
2) When $m_p < m_{up}$: Although the peened sample corrodes less and loses less mass, the corrosion rate still depends on the ratio of (m/A). Since the ratio of (m/A) is uncertain, it is difficult to compare the corrosion rates in this case.
3) When $m_p = m_{up}$, $\underline{r_p} < r_{up}$: If equal amounts of mass are lost between a peened and unpeened sample, the corrosion rate of a peened sample will be lower than the

corrosion rate of an unpeened sample because $(m/A)_p < (m/A)_{up}$. That is, A_p is greater than A_{up}.

Thus, it is essential to find the accurate mass loss of peened and unpeened magnesium to effectively compare the corrosion rates. These results indicate there is a distinction between the volume of material corroded and the rate at which it has corroded. Care should be taken when investigating the effect of surface treatments on the corrosion rate to distinguish between corrosion rate and volume (*i.e.*, mass lost).

6.2 Recommendations

6.2.1 Hydrogen Evolution Setup for Stress Corrosion Behavior Measurement

Potentiodynamic polarization (PDP) was used in this study to find the corrosion resistance of WE43. However, PDP gives only a comparative method to assess the initial corrosion behavior. Hydrogen evolution test can provide a more accurate measure of the long term corrosion behavior. An analogy to compare PDP and immersion is the difference between looking at a picture versus watching a movie. PDP provides a snapshot (*i.e.*, picture) of the instantaneous corrosion rate. Immersion is analogous to watching the movie in order to understand mass of material lost over time.

A hydrogen evolution test setup has been designed to find the corrosion rate of shot peened alloy in the absence of polarization. This stress corrosion setup will simulate more realistic physiological conditions. The setup consists of a magnesium sample stressed with the help of a tensile stress frame. A portion of magnesium sample is enveloped by the saline chamber to apply a corrosive environment. The assembly of stress frame, magnesium sample, and saline chamber is further sealed in an airtight container. The

airtight container is sealed at its point of contact with the saline chamber to avoid the damage of stress frame. The assembly of an airtight container (with saline chamber inside) is immersed in a glass tank of 0.5% NaCl solution. An inverted graduated beaker is placed over the saline chamber to collect hydrogen gas bubbles from the corrosion reaction of magnesium. The solution is covered with plastic balls or plastic wrap to avoid evaporation of solution. The solution inside the saline chamber is circulated with the help of a peristaltic pump. The solution is kept at a temperature of 37°C.

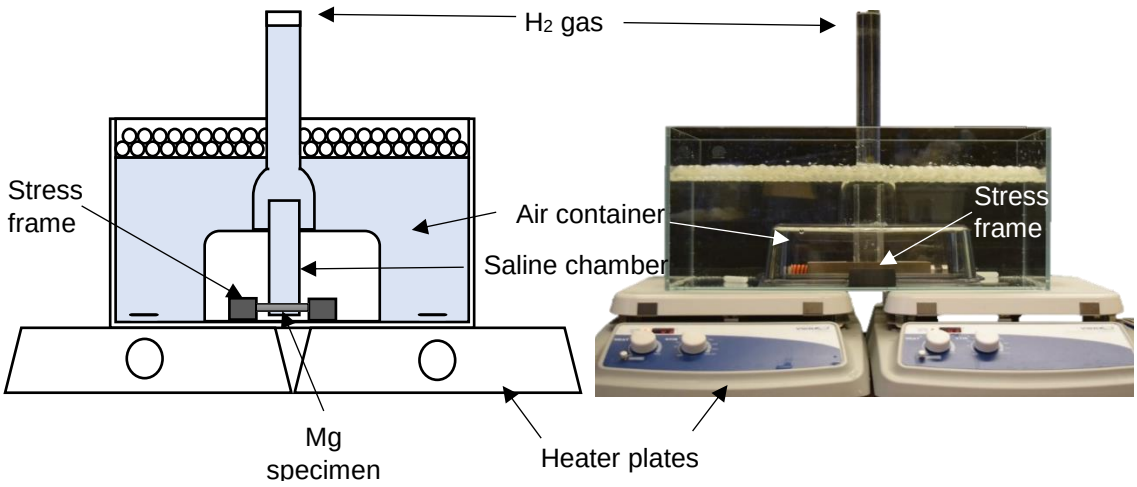

Fig. 6.1 Hydrogen evolution method arrangement for stress corrosion experiments.

6.2.2 Identify the Effect of Individual Surface Integrity Parameters on Corrosion

Surface integrity parameters, such as topography, microhardness, residual stresses contribute to the corrosion behavior of magnesium. In this study, it was observed that the combined effect of these parameters influenced the corrosion rate and the stress-corrosion rate of magnesium. However, the effect of individual surface integrity parameters on the

corrosion of magnesium is still unknown. It is necessary to identify the effect of individual surface integrity parameters to control the corrosion rate more efficiently.

6.2.3 Corrosion Fatigue Resistance

In this study, external tensile stress was applied to magnesium samples using a stress frame to simulate stress in an implant. However, both tensile and compressive forces are applied on an implant in physiological conditions. The type of stress imparted on a bone implant could be fatigue or a function of stress (*e.g.,* gait cycle). It is required to understand the effect of such complex stresses on the corrosion behavior of the alloy. Hence, the next step to this research could be analyzing the effect of fatigue on corrosion resistance of WE43.

6.2.4 Burnishing or Laser Shock Peening as a Surface Treatment

In this study, shot peening was used to induce surface residual stresses on the alloy. The peening pressure was measured from the pressure regulator on the shot peening machine, thus leading to inaccuracies in the pressure reading. Moreover, the shot flow during peening was found inconsistent, which could result in development of uneven residual stresses on the surface of the alloy. Due to these few drawbacks of shot peening, the manufacturing process of the part could have more errors. Thus, use of burnishing or laser shot peening could be considered for surface treating the alloy in future.

APPENDIX

04-013-4129 Feb 12, 2018 9:59 AM (svalloppilly2)

Status Primary **QM:** Star **Pressure/Temperature:** Ambient **Chemical Formula:** Mg **Empirical Formula:** Mg
Weight %: Mg100.00 **Atomic %:** Mg100.00 **Compound Name:** Magnesium

Radiation: CuKα1 **λ:** 1.5406 Å **d-Spacing:** Calculated **Intensity:** Calculated **I/Ic:** 3.85 **I/Ic - ND:** 0.99

SYS: Hexagonal **SPGR:** P63/mmc (194)
Author's Cell [AuthCell a: 3.2228(1) Å **AuthCell c:** 5.2191(2) Å **AuthCell Vol:** 46.95 Å³ **AuthCell Z:** 2.00
AuthCell MolVol: 23.48] **Author's Cell Axial Ratio [c/a:** 1.619]
Density [Dcalc: 1.719 g/cm³ **Dstruc:** 1.72 g/cm³] **SS/FOM:** F(26) = 309.8(0.0029, 29)
Temp: 298.0 K (Ambient temperature assigned by ICDD editor) **R-factor:** 0.079

Space Group: P63/mmc (194) **Molecular Weight:** 24.31
Crystal Data [XtlCell a: 3.223 Å **XtlCell b:** 3.223 Å **XtlCell c:** 5.219 Å **XtlCell α:** 90.00° **XtlCell β:** 90.00°
XtlCell γ: 120.00° **XtlCell Vol:** 46.95 Å³ **XtlCell Z:** 2.00]
Crystal Data Axial Ratio [c/a: 1.619 **a/b:** 1.000 **c/b:** 1.619]
Reduced Cell [RedCell a: 3.223 Å **RedCell b:** 3.223 Å **RedCell c:** 5.219 Å **RedCell α:** 90.00°
RedCell β: 90.00° **RedCell γ:** 120.00° **RedCell Vol:** 46.95 Å³]

Crystal (Symmetry Allowed): Centrosymmetric

SG Symmetry Operators:

Seq	Operator	Seq	Operator	Seq	Operator	Seq	Operator	Seq	Operator	Seq	Operator
1	x,y,z	5	-x+y,-x,z	9	x,x-y,z	13	-x,-y,z+1/2	17	x-y,x,z+1/2	21	-x,-x+y,z+1/2
2	-x,-y,-z	6	x-y,x,-z	10	-x,-x+y,-z	14	x,y,-z+1/2	18	-x+y,-x,-z+1/2	22	x,x-y,-z+1/2
3	-y,x-y,z	7	-y,-x,z	11	-x+y,y,z	15	y,-x+y,z+1/2	19	y,x,z+1/2	23	x-y,-y,z+1/2
4	y,-x+y,-z	8	y,x,-z	12	x-y,-y,-z	16	-y,x-y,-z+1/2	20	-y,-x,-z+1/2	24	-x+y,y,-z+1/2

Atomic Coordinates:

Atom	Num	Wyckoff	Symmetry	x	y	z	SOF	IDP	AET
Mg	1	2c	-6m2	0.33333	0.66666	0.25	1.0		

Subfile(s): Common Phase, Explosive, Forensic, Hydrogen Storage Materials, Inorganic, Metals & Alloys
Prototype Structure [Formula Order]: Mg **Prototype Structure [Alpha Order]:** Mg
LPF Prototype Structure [Formula Order]: Mg,hP2,194 **LPF Prototype Structure [Alpha Order]:** Mg,hP2,194
Pearson Symbol: hP2.00

Cross-Ref PDF #'s: 01-071-3765 (Alternate), 01-071-4618 (Alternate), 01-071-6543 (Alternate), 01-073-3812 (Alternate), 01-077-8460 (Alternate), 01-079-6692 (Alternate), 01-080-4430 (Alternate), 01-082-9643 (Alternate), 01-089-4894 (Alternate), 01-089-5003 (Alternate), 01-089-7195 (Alternate), ✓ 04-001-0208 (Alternate), ✓ 04-001-1763 (Alternate), ✓ 04-003-2174 (Alternate), ✓ 04-003-2526 (Alternate), ✓ 04-003-5036 (Alternate), ✓ 04-003-5224 (Alternate), ✓ 04-003-5226 (Alternate), ✓ 04-003-5290 (Alternate), ✓ 04-003-5619 (Alternate), ✓ 04-003-5621 (Alternate), ✓ 04-004-8048 (Alternate), ✓ 04-004-8053 (Alternate), ✓ 04-004-8054 (Alternate), ✓ 04-004-8745 (Alternate), ✓ 04-006-2605 (Alternate), ✓ 04-006-3740 (Alternate), ✓ 04-007-2050 (Alternate), ✓ 04-007-3847 (Alternate), ✓ 04-012-3404 (Alternate), ✓ 04-012-3405 (Alternate), ✓ 04-014-0191 (Alternate), ✓ 04-015-0339 (Alternate), ✓ 04-015-0486 (Alternate), ✓ 04-015-2580 (Alternate), ✓ 04-016-4869 (Alternate)

Entry Date: 09/01/2010 **Last Modification Date:** 09/01/2011 **Last Modifications:** Reflections

References:

Type	DOI	Reference
Primary Reference		Calculated from LPF using POWD-12++.
Structure		"Crystal structure of Mg0.65Sc0.35Dx deuterides studied by X-ray and neutron powder diffraction". Latroche M., Kalisvaart P., Notten P.H.L. J. Solid State Chem. 179, 3024,3032 (2006).

Database Comments: LPF Collection Code: 1420775. Sample Preparation: STARTINGMATERIALS: Mg0.65 Sc0.35 H0.75. COMPOUND PREPARATION: thermal desorption at 773 K. Unit Cell Data Source: Powder Diffraction.

d-Spacings (28) - Mg - 04-013-4129 (Stick, Fixed Slit Intensity) - Cu Kα1 1.54056 Å

2θ (°)	d (Å)	I	h	k	l	*	2θ (°)	d (Å)	I	h	k	l	*	2θ (°)	d (Å)	I	h	k	l	*
32.0413	**2.791030**	246	1	0	0		77.5022	1.230600	21	2	0	2		117.2858	0.902030	33	2	1	3	
34.3363	**2.609550**	267	0	0	2		81.3369	1.181990	17	1	0	4		123.0432	0.876317	20	3	0	2	
36.4765	**2.461200**	999	1	0	1		90.0811	1.088570	35	2	0	3		124.6341	0.869850	3	0	0	6	
47.6695	1.906160	139	1	0	2		93.8039	1.054910	10	2	1	0		134.3035	0.835865	13	2	0	5	
57.1122	1.611400	143	1	1	0		96.3099	1.034000	55	2	1	1		136.1097	0.830453	4	1	0	6	
62.8975	1.476380	148	1	0	3		98.8619	1.014030	34	1	1	4		139.7630	0.820334	9m	2	1	4	
67.0046	1.395510	19	2	0	0		103.9725	0.977683	31m	1	0	5		139.7630	0.820334	m	3	0	3	
68.3620	1.371070	139	1	1	2		103.9725	0.977683	m	2	1	2		145.8957	0.805700	8	2	2	0	
69.6903	1.348150	97	2	0	1		107.8410	0.953080	7	2	0	4								
72.3647	1.304770	18	0	0	4		111.7782	0.930342	12	3	0	0								

湖南恒博新材料有限公司

CHINA HUNAN HIGH BROAD NEW MATERIAL CO. LTD.

2412# Cell 2,No.4 Block,Panorama,70 Chezhan North Road,Changsha,China 410100

CERTIFICATE OF QUALITY

Invoice No.: 2016-HNHB-0117#

CHANGSHA CHINA September 19, 2016

Batch Number : 40610-1-1

THIS IS TO CERTIFY THE QUALITY AS FOLLOWS:

DESCRIPTION OF GOODS Magnesium alloy Plate				**Grade:** WE43		**Thickness:** 1mm			**Quantity:** 7 pieces	
Y	Nd	Zr	Gd	Cu	Mn	Ni	Fe	Tensile Strength (Mpa)	Elongation (%)	Yield Strength (Mpa)
4.0486%	2.4792%	0.5174%	1.1781%	0.0113%	0.0056%	0.0006%	0.0018	239	6.1%	162

CHINA HUNAN HIGH BROAD NEW MATERIAL CO. LTD.

Authorized Signature

REFERENCES

[1] Kammer, C., Aluminium-Zentrale, D., 2000. *Magnesium taschenbuch*, Aluminium-Verlag, ISBN: 3870172649

[2] Witte, F., 2010. The history of biodegradable magnesium implants: A review, Acta Biomaterialia, Vol 6, Issue 5, p. 1680-1692.

[3] Witte, F., Hort, N., Vogt, C., Cohen, S., Kainer, K.U., Willumeit, R., Feyerabend, F., 2008. Degradable biomaterials based on magnesium corrosion, Current Opinion in Solid State and Materials Science, Vol 12, Issues 5-6, p. 63-72.

[4] Witte, F., Feyerabend, F., Maier, P., Fischer, J., Störmer, M., Blawert, C., Dietzel, W., Hort, N., 2007. Biodegradable magnesium–hydroxyapatite metal matrix composites, Biomaterials, Vol 28, Issue 13, p. 2163-2174.

[5] Staiger, M.P., Pietak, A.M., Huadmai, J., Dias, G., 2006. Magnesium and its alloys as orthopedic biomaterials: A review, Biomaterials Vol 27, Issue 9, p. 1728-1734.

[6] Okuma, T., 2001, Magnesium and bone strength, Nutrition Vol 17, Issues 7-8, p. 679-680.

[7] Saris, N.L., Mervaala, E., Karppanen, H., Khawaja, J.A., Lewenstam, A., 2000. Magnesium: An update on physiological, clinical and analytical aspects, Clinica Chimica Acta, Vol 294, Issues 1-2, p. 1-26.

[8] Zeng, R., Dietzel, W., Witte, F., Hort, N., Blawert, C., 2008. Progress and Challenge for Magnesium Alloys as Biomaterials, Advanced Engineering Materials, Vol 10, Issue 8, p. B3-B14.

[9] Zheng, Y.F., Gu, X.N., Witte, F., 2014. Biodegradable metals, Materials Science and Engineering: R: Reports 77, p. 1-34.

[10] Yamamoto, A., Honma, R., Sumita, M., 1998. Cytotoxicity evaluation of 43 metal salts using murine fibroblasts and osteoblastic cells, Journal of Biomedical Materials Research, Vol 39, Issue 2, p. 331-340.

[11] Xin, Y., Huo, K., Tao, H., Tang, G., Chu, P.K., 2008. Influence of aggressive ions on the degradation behavior of biomedical magnesium alloy in physiological environment, Acta Biomaterialia, Vol 4, Issue 6, p. 2008-2015.

[12] Janning, C., Willbold, E., Vogt, C., Nellesen, J., Meyer-Lindenberg, A., Windhagen, H., Thorey, F., Witte, F., 2010. Magnesium hydroxide temporarily enhancing osteoblast activity and decreasing the osteoclast number in peri-implant bone remodelling, Acta Biomaterialia,Vol 6, Issue 5, p. 1861-1868.

[13] Li, Z., Gu, X., Lou, S., Zheng, Y., 2008. The development of binary Mg–Ca alloys for use as biodegradable materials within bone, Biomaterials, Vol 29, Issue 10, p. 1329-1344.

[14] Kirkland, N.T., Birbilis, N., Staiger, M.P., 2012. Assessing the corrosion of biodegradable magnesium implants: A critical review of current methodologies and their limitations, Acta Biomaterialia, Vol 8, Issue 3, p. 925-936.

[15] Song, G., Atrens, A., 2003. Understanding Magnesium Corrosion—A Framework for Improved Alloy Performance, Advanced Engineering Materials, Vol 5, Issue 12, p. 837-858.

[16] Guo, Y., Sealy, M.P., Guo, C., 2012. Significant improvement of corrosion resistance of biodegradable metallic implants processed by laser shock peening, CIRP Annals,Vol 61, Issue 1, p. 583-586.

[17] Zhang, Y., You, J., Lu, J., Cui, C., Jiang, Y., Ren, X., 2010. Effects of laser shock processing on stress corrosion cracking susceptibility of AZ31B magnesium alloy, Surface and Coatings Technology, Vol 204, Issue 24, p. 3947-3953.

[18] Sealy, M., Liu, Z., Li, C., Guo, Y., White, B., 2017. A Strategy to Optimize Recovery in Orthopedic Sports Injuries, J Bioanal Biomed, Vol 9, Issue (3), p. 144-151.

[19] Seal, C.K., Vince, K., Hodgson, M., 2009. Biodegradable surgical implants based on magnesium alloys–A review of current research, Vol 4, p. 012011.

[20] Fraunhofer Institute for Laser Technology (ILT, Aachen, G., . https://www.industrial-lasers.com/articles/2016/03/selective-laser-melting-method-works-with-magnesium-alloys.html.

[21] Magmaris Resorbable Magnesium Scaffold, . https://www.biotronik.com/en-fi/products/vi/coronary/magmaris.

[22] Syntellix MAGNEZIX, . http://www.syntellix.de/produkte/produktuebersicht/alle.html.

[23] U&I Corporation, . http://www.youic.com/sub02/list.php.

[24] nanoMAG, . http://www.nanomag.us/products.html, http://www.nanomag.us/pdfs/nanoMAG_BioMg_In_Vivo.pdf.

[25] Zheng, Y.F., Gu, X.N., Witte, F., 2014. Biodegradable metals, Materials Science and Engineering: R: Reports 77, p. 1-34.

[26] Witte, F., Hort, N., Vogt, C., Cohen, S., Kainer, K.U., Willumeit, R., Feyerabend, F., 2008. Degradable biomaterials based on magnesium corrosion, Current Opinion in Solid State and Materials Science, Vol 12, Issues 5-6, p. 63-72.

[27] Song, G., 2007. Control of biodegradation of biocompatable magnesium alloys, Corrosion Science, Vol 49, Issue 4, p. 1696-1701.

[28] Wagner, L., 1999. Mechanical surface treatments on titanium, aluminum and magnesium alloys, Materials Science and Engineering, Vol 263, Issue 2, p. 210-216.

[29] Sealy, M.P., Guo, Y.B., 2010. Surface integrity and process mechanics of laser shock peening of novel biodegradable magnesium–calcium (Mg–Ca) alloy, Journal of the Mechanical Behavior of Biomedical Materials, Vol 3, Issue 7, p. 488-496.

[30] Guo, Y., Sealy, M.P., Guo, C., 2012. Significant improvement of corrosion resistance of biodegradable metallic implants processed by laser shock peening, CIRP Annals - Manufacturing Technology, Vol 61, Issue 1, p. 583-586.

[31] Li, X.C., Zhang, Y.K., Chen, J.F., Lu, Y.L., 2013. Effect of laser shock processing on stress corrosion cracking behaviour of AZ31 magnesium alloy at slow strain rate, Materials Science and Technology, Vol 29, Issue 5 p. 626-630.

[32] Kamkarrad, H., Narayanswamy, S., Tao, X.S., 2014. Feasibility study of high-repetition rate laser shock peening of biodegradable magnesium alloys, The International Journal of Advanced Manufacturing Technology, Vol 74, Issue 9-12, p. 1237-1245.

[33] Mhaede, M., Pastorek, F., Hadzima, B., 2014. Influence of shot peening on corrosion properties of biocompatible magnesium alloy AZ31 coated by dicalcium phosphate dihydrate (DCPD), Materials Science and Engineering: C, Vol 39, p. 330-335.

[34] Hadzima, B., Bukovina, M., Doležal, P., 2010. Shot peening influence on corrosion resistance of AE21 magnesium alloy, Materials Engineering, Vol 14, Issue 4, p. 14.

[35] Zhang, P., Lindemann, J., Leyens, C., 2010. Shot peening on the high-strength wrought magnesium alloy AZ80—Effect of peening media, Journal of Materials Processing Technology, Vol 210, Issue 3, p. 445-450.

[36] Pu, Z., Yang, S., Song, G.-., Dillon, O.W., Puleo, D.A., Jawahir, I.S., 2011. Ultrafine-grained surface layer on Mg–Al–Zn alloy produced by cryogenic burnishing for enhanced corrosion resistance, Scripta Materialia, Vol 65, Issue 6, p. 520-523.

[37] Pu, Z., Song, G., Yang, S., Outeiro, J.C., Dillon, O.W., Puleo, D.A., Jawahir, I.S., 2012. Grain refined and basal textured surface produced by burnishing for improved corrosion performance of AZ31B Mg alloy, Corrosion Science, Vol 57, p. 192-201.

[38] Hoche, H., Scheerer, H., Probst, D., Broszeit, E., Berger, C., 2003. Development of a plasma surface treatment for magnesium alloys to ensure sufficient wear and corrosion resistance, Surface and Coatings Technology, Vol 174-175, p. 1018-1023.

[39] Forsyth, M., Howlett, P.C., Tan, S.K., MacFarlane, D.R., Birbilis, N., 2006. An ionic liquid surface treatment for corrosion protection of magnesium alloy AZ31, Electrochemical and solid-state letters, Vol 9, Issue 11, p. B52-B55.

[40] Gérrard Eddy Jai Poinern, Sridevi Brundavanam, Derek Fawcett, 2012. Biomedical Magnesium Alloys: A Review of Material Properties, Surface Modifications and Potential as a Biodegradable Orthopaedic Implant, American Journal of Biomedical Engineering, Vol. 2, Issue 6, p. 218-240.

[41] Winzer, N., Atrens, A., Song, G., Ghali, E., Dietzel, W., Kainer, K. , Hort, N., Blawert, C., 2005. A Critical Review of the Stress Corrosion Cracking (SCC) of Magnesium Alloys, Advanced Engineering Materials, Vol 7, Issue 8, p. 659-693.

[42] Sozańska, M., Mościcki, A., Chmiela, B., 2017. Investigation of Stress Corrosion Cracking in Magnesium Alloys by Quantitative Fractography Methods, Archives of Metallurgy and Materials, Vol 62, Issue 2, p. 557-562.

[43] Yu, Z., Ju, D., Zhao, H., 2013. Effect of stress corrosion cracking at various strain rates on the electrochemical corrosion behavior of Mg-Zn-In-Sn alloy, Journal of Environmental Sciences, Vol 25, Supplement 1, p. S50-S53.

[44] Wang, S., Xu, D., Wang, B., Sheng, L., Han, E., Dong, C., 2016. Effect of solution treatment on stress corrosion cracking behavior of an as-forged Mg-Zn-Y-Zr alloy, Scientific reports, Vol 6, p. 29471.

[45] D. Jones, 1996. Environmentally induced cracking, in *Principles and prevention of corrosion* Anonymous, ISBN 1292042559, p. 279-285.

[46] Wu, L., Wang, W., Hsu, Y., Trong, S., 2007. Effects of microstructure on the mechanical properties and stress corrosion cracking of an Al-Zn-Mg-Sc-Zr alloy by various temper treatments, Materials transactions, Vol 48, Issue 3, p. 600-609.

[47] Chang, P., Chen, C., Chao, C., 2016. Effect of Microstructure Factors on Stress Corrosion Behavior of Mg-xSn Alloys (x= 2, 5, 8 mass%), Materials transactions Vol 57, Issue 3, p. 1498-1504.

[48] Li, S., Chen, Z., Tan, L., Bobaru, F., 2018. Corrosion-induced embrittlement in ZK60A Mg alloy, Materials Science and Engineering: A, Vol 713, p. 7-17.

[49] De Meo, D., Diyaroglu, C., Zhu, N., Oterkus, E., Siddiq, M.A., 2016. Modelling of stress-corrosion cracking by using peridynamics, International Journal of Hydrogen Energy, Vol 41, Issue 15, p. 6593-6609.

[50] Silling, S.A., 2000. Reformulation of elasticity theory for discontinuities and long-range forces, Journal of the Mechanics and Physics of Solids, Vol 48, Issue 1, p. 175-209.

[51] Chen, Z., Bobaru, F., 2015. Peridynamic modeling of pitting corrosion damage, Journal of the Mechanics and Physics of Solids, Vol 78, p. 352-381.

[52] Chen, Z., Zhang, G., Bobaru, F., 2016. The influence of passive film damage on pitting corrosion, Journal of the Electrochemical Society, Vol 163, Issue 2, p. C19-C24.

[53] Michael P. Sealy, 2014. Processing, surface integrity, and performance of biodegradable magnesium-calcium implants by laser shock peening, Dissertation Chapter 4, p. 55.

[54] Champaigne, J., 2001. Shot peening overview, Metal Improvement Company. www.shotpeener.com

[55] Tobben, H., 1999. Select the Best Nozzle for Cost-Effective Shot Peening, The Shot Peener, Vol 13, p. 1-3.

[56] I'Anson, K., 1992. The Shot Peener Workshop on Shot Peening, Cincinatti, Ohio, Blastworks Inc., The Shot Peener, p. 1-20.

[57] Kieswetter, K., Schwartz, Z., Dean, D., Boyan, B., 1996. The role of implant surface characteristics in the healing of bone, Critical Reviews in Oral Biology & Medicine, Vol 7, Issue 4, p. 329-345.

[58] Bagherifard, S., Hickey, D.J., de Luca, A.C., Malheiro, V.N., Markaki, A.E., Guagliano, M., Webster, T.J., 2015. The influence of nanostructured features on bacterial adhesion and bone cell functions on severely shot peened 316L stainless steel, Biomaterials, Vol 73, p. 185-197.

[59] Kirk, D., Abyaneh, M., 1995. Theoretical basis of shot peening coverage control, Shot Peener(USA), Vol 9, Issue 2, p. 28-30.

[60] Prevéy, P.S., 2001. X-ray diffraction characterization of residual stresses produced by shot peening, Shot Peener(USA), Vol 15, p. 4-8.

[61] Prevéy, P.S., 1990. X-ray diffraction characterization of residual stresses produced by shot peening.

[62] Fitzpatrick, M., Fry, A., Holdway, P., Kandil, F., Shackleton, J., Suominen, L., 2005. Determination of residual stresses by X-ray diffraction, ISSN 1368-6550

[63] Witte, F., Kaese, V., Haferkamp, H., Switzer, E., Meyer-Lindenberg, A., Wirth, C.J., Windhagen, H., 2005. In vivo corrosion of four magnesium alloys and the associated bone response, Biomaterials, Vol 26, Issue 17, p. 3557-3563.

[64] Witte, F., Fischer, J., Nellesen, J., Crostack, H., Kaese, V., Pisch, A., Beckmann, F., Windhagen, H., 2006. In vitro and in vivo corrosion measurements of magnesium alloys, Biomaterials, Vol 27, Issue 7, p. 1013-1018.

[65] Kirkland, N.T., Birbilis, N., Staiger, M.P., 2012. Assessing the corrosion of biodegradable magnesium implants: A critical review of current methodologies and their limitations, Acta Biomaterialia, Vol 8, Issue 3, p. 925-936.

[66] Dauphin-Ducharme, P., Mauzeroll, J., 2015, Surface analytical methods applied to magnesium corrosion, American Chemical Society, Vol 87, Issue 15, p. 7499-7509

[67] Esmaily, M., Svensson, J., Fajardo, S., Birbilis, N., Frankel, G., Virtanen, S., Arrabal, R., Thomas, S., Johansson, L., 2017. Fundamentals and advances in magnesium alloy corrosion, Progress in Materials Science, Vol 89, p. 92-193.

[68] Bland, L., King, A., Birbilis, N., Scully, J., 2014. Assessing the corrosion of commercially pure magnesium and commercial AZ31B by electrochemical impedance, mass-loss, hydrogen collection, and inductively coupled plasma optical emission spectrometry solution analysis, Corrosion, Vol 71, Issue 2, p. 128-145.

[69] Birbilis, N., King, A., Thomas, S., Frankel, G., Scully, J., 2014. Evidence for enhanced catalytic activity of magnesium arising from anodic dissolution, Electrochimica Acta, Vol 132, p. 277-283.

[70] Elsentriecy, H.H., Azumi, K., Konno, H., 2008. Effects of pH and temperature on the deposition properties of stannate chemical conversion coatings formed by the potentiostatic technique on AZ91 D magnesium alloy, Electrochimica Acta, Vol 53, Issue 12, p. 4267-4275.

[71] Rybalka, K., 2014. Determination of metal corrosion rate using the pH-metry by the method of compensating additives, Russian Journal of Electrochemistry, Vol 50, Issue 5, p. 500-502.

[72] Yang, H., Zhang, Q., Tu, S., Wang, Y., Li, Y., Huang, Y., 2016. A study on time-variant corrosion model for immersed steel plate elements considering the effect of mechanical stress, Ocean Engineering, Vol 125, p. 134-146.